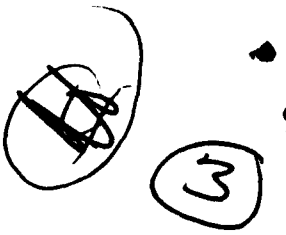

ANNUAL REPORT

to the

OFFICE OF NAVAL RESEARCH

for

ADVANCED LASER SOURCE RESEARCH

N00014-91-J-1023
R&T 4124100

10/01/93 - 09/30/94

# # #

Principal Investigator: Richard N. Zare
Marguerite Blake Wilbur Professor of Chemistry

Co-Principal Investigator: Stephen E. Harris
Professor of Electrical Engineering and Applied Physics

Co-Principal Investigator: Arthur L. Schawlow
J.G. Jackson-C.J. Wood Professor of Physics

R&T 4124100
Contract N00014-91-J-1023
Office of Naval Research

ADVANCED LASER SOURCE RESEARCH

Annual Report for the Period
10/1/93 - 9/30/94

Principal Investigator:
S. E. Harris

Edward L. Ginzton Laboratory
Stanford University
Stanford, CA 94305

July 1994

Contract Monitor:
Dr. Herschel S. Pilloff
ONR 331
Chemistry and Physics Division
Science and Technology Department
Office of Naval Research
800 N. Quincy Street
Arlington, VA 22217-5660

INTRODUCTION

To some extent, this has been a year of building and results have come together only within the last month. We now have a laser system which allows us to observe electromagnetically induced transparency in regions never before accessible. Briefly, the system produces two wavelengths (i.e., 406 nm and 283 nm), each with a frequency stability of several MHz and with energy of several mJ. One laser has a pulsewidth of about 100 ns, while the other has a pulsewidth of 2 ns; both are tunable over about 60 GHz.

Using this system, we are now able to observe an increase in transparency of over a factor of 10,000 in an exponent. We also observe optical group velocities as slow as c/100. We are beginning the observation and study of large signal effects. In this regime there is a modification of group velocity and substantial reshaping of both laser pulses. The most exciting result is about a week old: Once the transparency is created, we observe a diffraction pattern almost identical to that of the probe laser propagating in high vacuum. Without the control laser present, the probe laser beam is temporally and spatially unstable and, on successive shots, moves by three or four spot sizes. In the presence of the controlling laser, the probe laser beam is clear and stable.

The other important area of work this year has been the identification of the normal modes of electromagnetically induced transparency. These modes follow from the basic properties of this effect, wherein the electromagnetic field creates population-trapped atoms and where population-trapped atoms produce matched pulses. The key idea is to use field variables which are the sum and difference of the field envelopes at the

controlling and probe laser frequencies. To establish either of the normal modes, one applies either matched or anti-matched pulses at $z=0$.

The following sections give further details of progress under this contract. We note that this work has been jointly supported by the Air Force Office of Scientific Research and the Army Research Office.

A. LASER SYSTEMS FOR ELECTROMAGNETICALLY INDUCED TRANSPARENCY EXPERIMENTS

(A. Kasapi and M. Jain)

1. REQUIREMENTS

We have chosen Pb vapor as the prototype system for many of our experiments on EIT, slow group velocities, nonlinear optics with EIT, and lasers without inversion. Pb vapor was chosen since both the coupling and probe wavelengths could be generated using high-quality Ti:Sapphire lasers. Specifically, we require:

(1) High power density (up to 10^8 W/cm^2).

(2) A near-Gaussian spatial mode.

(3) Temporally smooth pulse envelopes with no phase noise.

(4) Absolute frequency stability to within a few MHz and tunability of about 1 cm^{-1}.

The wavelengths of the coupling and probe lasers are 406 nm and 283 nm. These wavelengths are obtained by frequency doubling and tripling, respectively, Ti:Sapphire lasers at 812 nm and 850 nm. These systems are now fully operational and are described in detail below.

2. DESCRIPTION OF THE LASER SYSTEMS

Each laser system consists of a continuous wave master oscillator seeding a pulse-pumped Ti:Sapphire ring laser. Figure 1 shows a schematic of each of the Ti:Sapphire lasers.

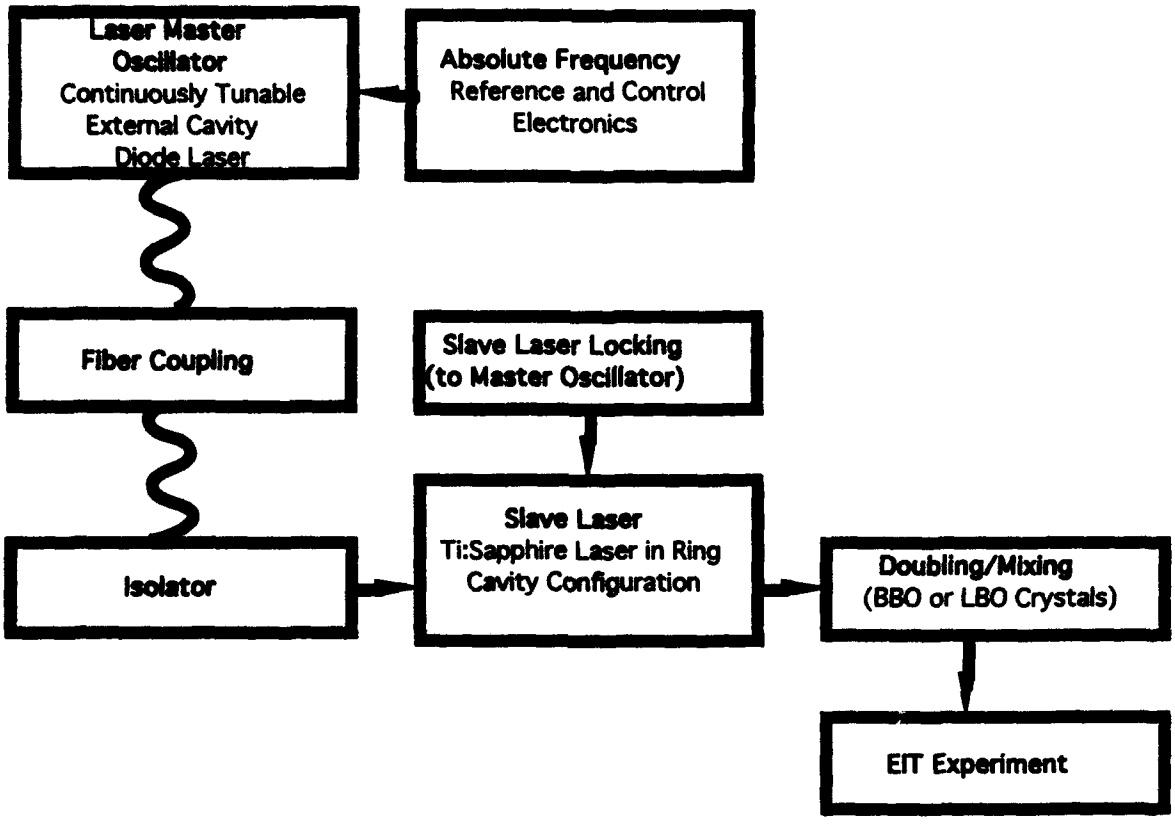

Fig. 1. Block diagram of Ti:Sapphire lasers.

3. MASTER OSCILLATOR

The master oscillator for each laser system is an external cavity stabilized diode laser. The external cavity is in the Littman configuration, which consists of a grazing incidence diffraction grating and an end mirror.

The laser is continuously tunable over a range of 30 GHz by pivoting the end mirror as shown in Fig 2. The addition of a low voltage piezoelectric stack to the lever arm allows for automated electronic tuning by the frequency reference electronics.

Both diode laser assemblies (one for the 812-nm system and one for the 850-nm system) have been mechanically constructed to be especially insensitive to external vibrations. In addition, the cavities are acoustically shielded and the optical table employs pneumatic legs to dampen table oscillations. The dominant source of noise in the cavity, however, is still mechanical in nature: random vibrations.

The diodes are thermally stabilized by commercial temperature controllers and thermoelectric coolers, and we are able to obtain stabilized laser power at approximately 25% of the rated diode laser power. However, any index-guided diode laser may be used for the assembly and, since the external cavity greatly reduces the effect of current noise on the diode source, a common commercial current source is used.

The unlocked lasers drift approximately 1 GHz per hour and have a short-term linewidth of less than 1 MHz.

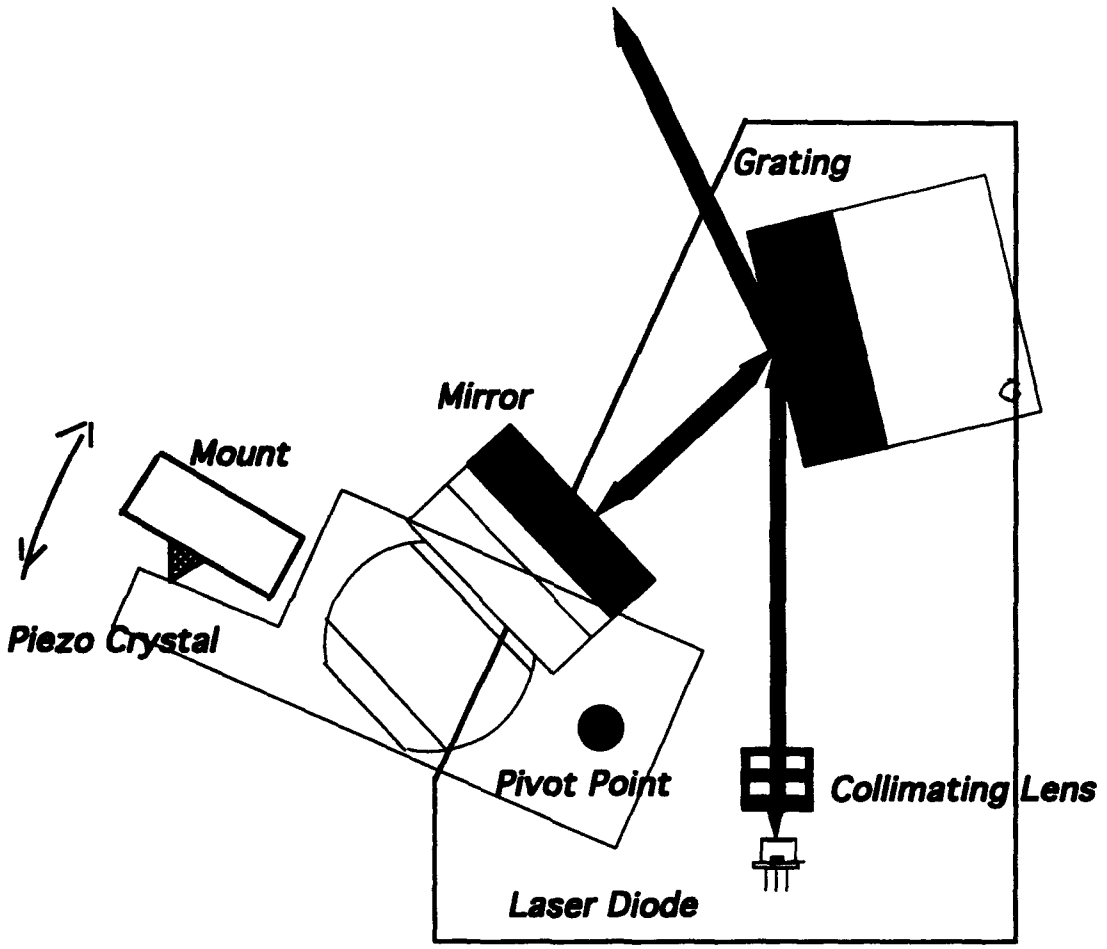

Fig. 2. Littman laser arrangement.

4. FREQUENCY REFERENCE AND CONTROL ELECTRONICS

In order to maintain absolute frequency stability to within a few MHz, the master oscillators are locked to temperature-stabilized quartz etalons. The temperature of the etalon is controlled by a commercial temperature controller/thermistor combination to within 1 mK. The technique of offset locking allows us to lock the master oscillators to any desired point on the etalon line spectra.

Offset locking works as follows. A portion of the master oscillator output is split into two paths by a beamsplitter; the temperature-controlled etalon is placed in one path, while the other path is left empty. Photodetectors are placed at the end of each path. The difference signal from the two photodetectors is amplified by a proportional/integral gain circuit and the angle of the master oscillator cavity mirror is continually adjusted by feeding this difference signal into the piezoelectric stack mounted on the mirror lever. The point on the etalon line spectrum to which we lock may be changed by providing one of the photodetector arms with variable gain before generating the difference signal.

The temperature of the quartz etalon must be controlled as precisely as possible because both the length and the refractive index of the quartz etalon are functions of temperature. The etalon temperature has on order 1 mK temperature variation and, as a result, we are only able to stabilize the peak of the etalon to within 3 MHz; however, this level of frequency stability is sufficient for our purposes.

5. FIBER COUPLING

The output of the laser master oscillators is propagated to the slave laser assembly through roughly 30 feet of commercial,

non-polarization-preserving, 6 μm glass core fiber. This fiber coupling serves two purposes. First, it acts as a "beam scrubber," producing a spatial Gaussian beam from the highly astigmatic, spatial beam emitted by the diode laser. The slave laser is far easier to align using a clean seed beam than with the native diode beam and we thus require less seed power to seed the laser.

Secondly, the fiber allows us to decouple the alignment of the slave laser from the alignment of the master oscillator; since the output end of the fiber remains fixed, the master seed beam always comes from a fixed direction. We are thus able to separately align the two laser systems without disturbing the overall coupling. In addition, the master oscillator and slave lasers are subject to different vibration and motions; without the decoupling provided by the fiber, we could not reliably seed the slave laser.

6. ISOLATOR

The isolator is required to protect the diode laser and fiber coupling against pulses from the slave laser which propagate backwards toward the diode laser. It was found that, when even a few milliwatts of power from these pulses reach the diode laser, all stability is lost in the master oscillator.

When seeding is effective, lasing in the slave cavity is unidirectional and there is no danger of such a pulse. If, however, the seeding is momentarily lost, lasing occurs in both directions and a backward pulse is sent toward the master oscillator. In order to eliminate these pulses, we include two Faraday isolators in series, each of which provides 35 dB of reverse rejection. The isolators are commercially available units constructed of TGG glass, fixed magnets, and calcite polarizers.

7. SLAVE LASER

The slave laser assembly is a gain-switched, Ti:Sapphire laser arranged in a ring geometry, as shown schematically in Fig 3.

The gain medium is a highly-doped commercial sapphire crystal, cut so that the c-axis is coincident with p-polarization for Brewster's angle at the input and output faces. The pump laser beam is a 5-ns-long pulse of 532 nm radiation produced by doubling the 1064 *nm* output of a commercial pulsed-YAG laser system. Each YAG laser has been modified to produce a "filled-in" beam mode, rather than the native donut-mode, so that a more nearly uniform gain region in the crystal could be produced.

The intra-cavity Faraday rotator, polarizer, and half-waveplate minimize the amount of backward lasing in the slave laser. However, the residual backward lasing necessitates the presence of the external isolator assembly.

The slave laser is seeded by the master oscillator through the output coupler mirror as shown in Fig 3. When the cavity is on-resonance with the seed beam, the intracavity power of the seed beam is highest, and this power is monitored by a photodiode placed behind one of the high-reflectance (HR) mirrors. The cavity length is constantly adjusted by a piezoelectric transducer mounted behind the other HR mirror to maintain cavity resonance.

7.1 Slave Laser Locking

The technique employed to lock the slave laser oscillator to the master oscillator is somewhat different from the one used to lock the master oscillator to the frequency reference.

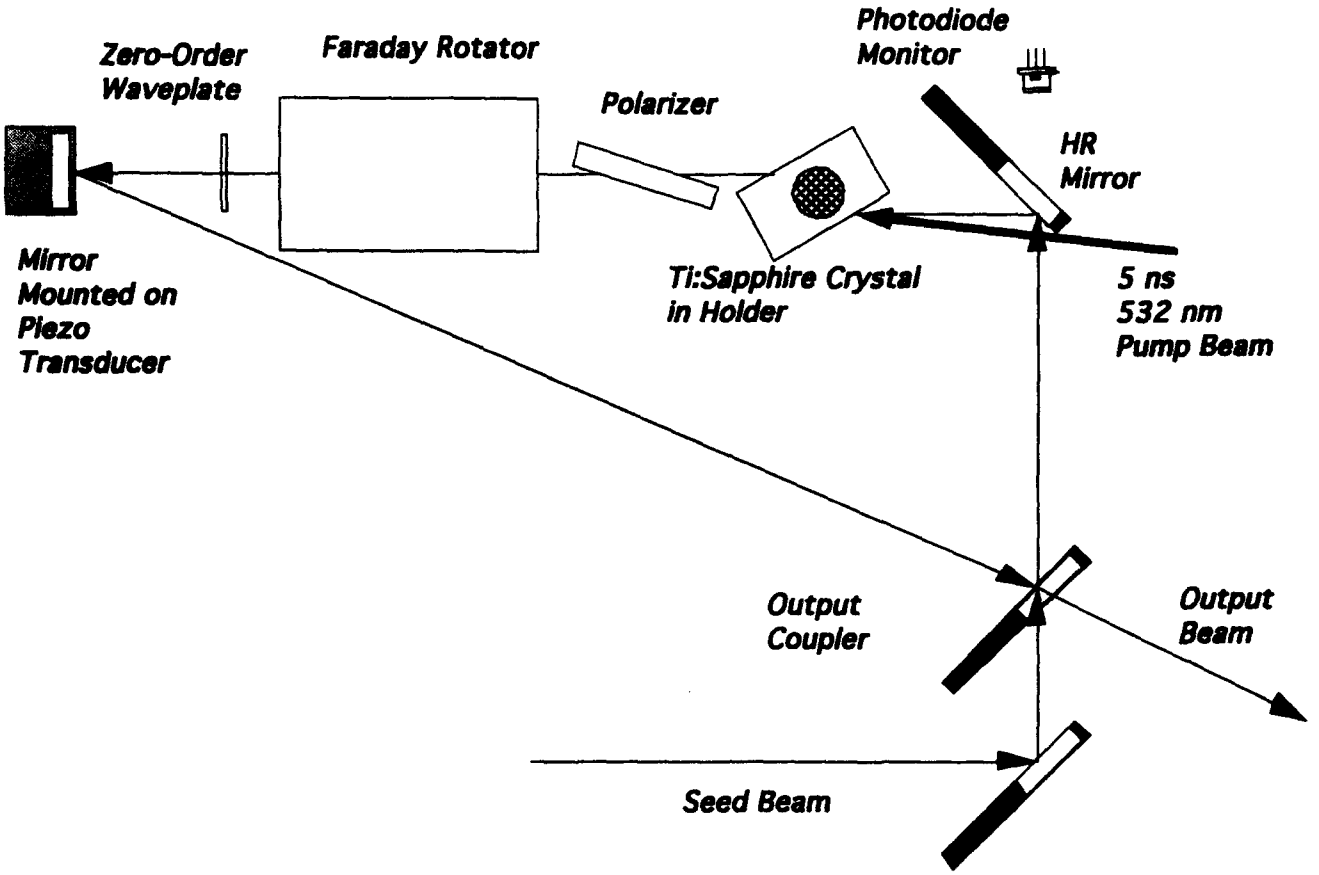

Fig. 3. Ti:Sapphire slave laser system.

The master oscillator is frequency dithered by superimposing a few milliamp amplitude, 10 kHz drive signal onto the 80 mA laser diode power supply. This dithering produces a 10 kHz modulation of the slave laser cavity output, unless the slave cavity is centered at the master oscillator frequency. When centered, the output at the dither frequency disappears and is replaced by frequencies at the second harmonic. A lock-in amplifier connected to the output of the photodetector sitting behind the HR mirror is used to detect the output signal from the slave laser cavity at the dither frequency. The output of the lock-in amplifier is then fed into a proportional gain circuit and, finally, to the cavity mirror piezo-driver. The slave laser cavity is thus locked to the laser master oscillator.

7.2 850-nm Slave Laser Modifications

The gain profile of the Ti:Sapphire crystal peaks at roughly 800 nm. Hence, the cavity will lase effectively, without modification, when seeded by the 812 nm radiation. However, we found that the 850 nm seeding did not result in single frequency slave cavity lasing. Therefore, a frequency-selective element had to be introduced into the cavity of the 850 nm laser system. Prism tuning was first utilized with a fused silica Pellin-Broca prism, but rejected on the basis that it did not allow for the generation of stable short pulses. We have since, however, successfully implemented birefringent tuning using a combination of waveplates and polarizing materials. Birefringent tuning escapes its predecessor's problems because its frequency selectivity does not depend upon the cavity size. Single-mode lasing at 850 nm has thus been achieved.

8. DOUBLING AND TRIPLING

To efficiently double the light at 812 nm, a barium borate (BBO) crystal is used. This type of crystal is useful for nonlinear optical generation because of its high nonlinear coefficients, but it also causes significant beam walkoff. Thus, if the fundamental beam is focused tightly on the BBO crystal, the output at 2ω has an elliptical spatial profile which can be corrected by an appropriate prism pair. We have achieved conversion efficiencies of roughly 30% using Type I, angle-tuned phasematching and fundamental intensities on the order of 100 MW/cm^2.

The 850 nm radiation must be tripled to 283 nm for use in our experiments. This is accomplished by first doubling the 850 nm and then mixing the fundamental and the doubled frequency to obtain radiation at 3ω. The fundamental is doubled using a LBO crystal instead of the BBO crystal. The LBO crystal has a much smaller walkoff than the BBO crystal, so that the 2ω output still has a circular spatial profile. As a result of the Type I phasematching in the LBO crystal, the doubled light is polarized orthogonally to the fundamental and we can then directly mix the two beams using Type II phasematching in a BBO crystal. However, we have chosen mixing utilizing Type I phasematching because of the much higher nonlinearities (roughly five times greater than Type II). To accomplish this, we insert a waveplate which preserves the polarization of the 850 nm radiation, but which rotates the 425 nm polarization by 90^o, so that the two input beams are polarized in the same direction. This results in a net 3ω generation conversion efficiency on the order of a few percent.

9. STATUS AND FUTURE MODIFICATIONS

Figure 4 shows a schematic of the overall laser system at 850 nm. This laser system and a similar one at 812 nm are currently being used in demonstrating slow group velocity and large signal EIT effects in Pb vapor. Table 1 details the present status of this system.

As we proceed toward performing experiments in nonlinear optical frequency-mixing in Pb vapor, some slight modifications to the laser systems will be necessary. We will need an optical Ti:Sapphire amplifier at 812 nm to increase the coupling laser (406 nm) Rabi frequency to carry out these experiments. An amplifier for the 850 nm laser may also be necessary. It is expected that the present absolute frequency stability of the laser systems will be sufficient for these experiments. Next, for the VUV generation experiment in Kr, we need to make only minor changes to the 850-nm laser system, but will need to replace the 812-nm system with a system at 760 nm. This can easily be achieved by replacing the laser diode at 812 nm with one at 760 nm and, perhaps, with the addition of an intracavity tuning element in the present regenerative cavity. Hence, the proposed experiments may be carried out with some changes to existing laser systems.

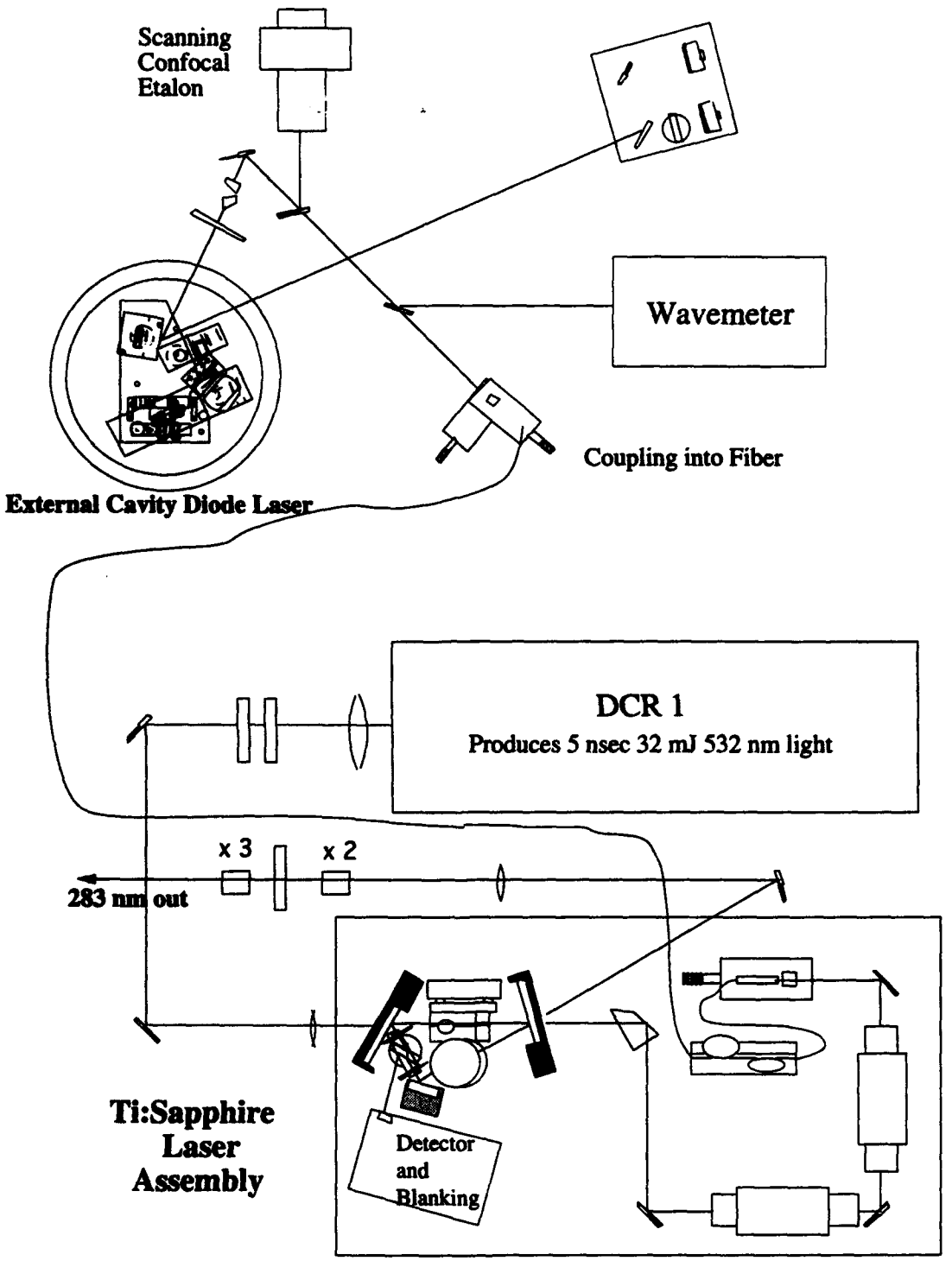

Fig. 4. Ti:Sapphire laser system with frequency-stabilized injection seeding.

Table 1. Comparison of desired and actual laser system performance.

Parameter	Desired Value	Actual Value	Notes
Pulsewidth	406 nm: 100 ns 283 nm: 14 ns	100 ns 14 ns	Doubled 812 nm Tripled 850 nm
Pulse Jitter	0 ns	20 - 40 ns	Due to 5% shot-to-shot variation of pump laser energy
Frequency Stability	3 MHz over few hours	15 MHz over 3 days Measured	These values are at the fundamental frequencies
Linewidth	3 MHz	3-5 MHz Estimated	Fourier Transform Limited.
Pulse Energy	5 - 10 mJ/pulse	5 mJ	
Power Density	near IR: $> 10^6$ W/cm^2	up to 10^8 W/cm^2	Required for efficient generation of 2ω and 3ω radiation
Tunability	60 GHz	> 60 GHz	30 GHz tuning in master oscillator (which is doubled)
Pulse Repetition Rate	10 Hz	10 Hz	

B. OBSERVATION OF SLOW GROUP VELOCITIES

(A. Kasapi and M. Jain)

Electromagnetically induced transparency (EIT) experiments to date have clearly demonstrated transparency, as seen by a probe tuned on line-center. Here, we report the first experimental results which study the real part of the linear susceptibility. In particular, we have studied the steep slope of the refractive index at line center, which leads to slow group velocities of a probe pulse. We have observed dramatic changes in the group velocity of pulse propagation due to EIT. The experiment was carried out in Pb vapor and we observed group velocity delays of several pulsewidths for a weak probe at 283 nm, induced by the co-existent coupling laser at 406 nm. An energy level diagram of atomic Pb is shown in Fig. 1.

The weak 283-nm probe beam was co-propagated (with spatial and temporal overlap) with the 406-nm coupling laser. At the center of the 4-inch Pb vapor cell, the diameter of the probe beam was 300 μm and the coupling laser was 3 mm in diameter. The coupling laser pulsewidth was about 100 ns and the probe had a pulsewidth of about 2 ns. These two conditions ensured that the probe effectively sampled a fairly constant coupling laser, both spatially and temporally. Thus, our experimental conditions were close to the theoretical model. The 14-ns pulse output from the 283-nm Ti:Sapphire laser system was pulse shaped to about 2 ns using an electro-optic modulator driven by a short-pulse, high-voltage supply. This small probe pulsewidth allowed the clear resolution of group velocity delays which were several probe pulsewidths. The data was taken at a measured cell density of $N = 1.5 \times 10^{14} / cm^3$. This was measured by the curve of growth technique.

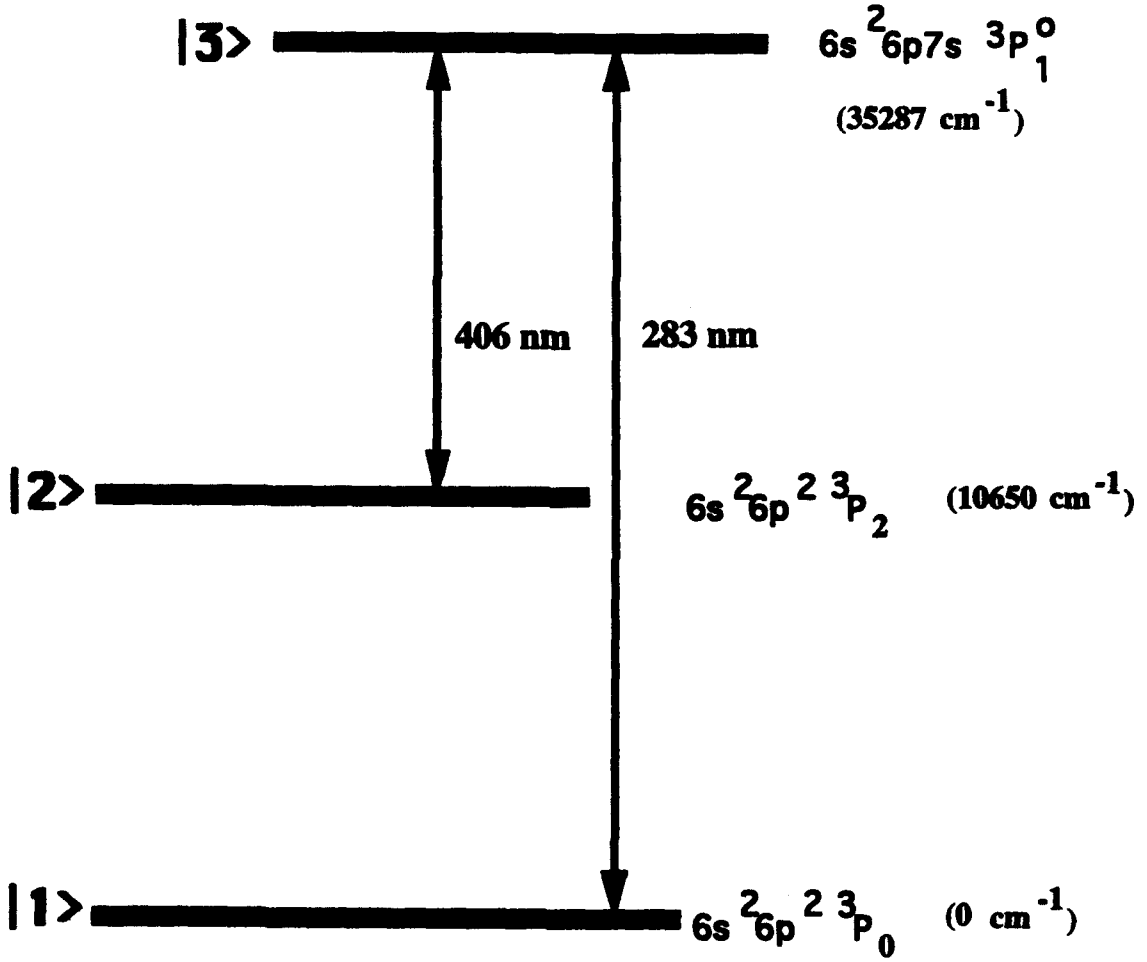

Fig. 1. Energy level diagram for slow group velocity experiment in Pb.

Figure 2 shows the dramatic results of this experiment. The pulse centered at 0 ns is the input probe pulse to the cell measured by a fast photodiode monitoring one of the beam-split components of the probe input to the Pb cell. The two pulses to the right were recorded by another fast photodiode measuring the output pulses from the cell. The cable delays for the two photodiodes were chosen so that a pulse going through the cold cell would appear centered at the 0-ns mark for both the input and output photodiodes. The pulse centered around the 10-ns mark indicates a group velocity slowdown of about c/31 and has a measured transmission through the 4-inch cell of about 30%. This pulse corresponds to a probe Rabi frequency of 0.02 cm^{-1} and a coupling laser Rabi frequency of 0.3 cm^{-1}. The second output pulse (centered near 18 ns) indicates a group velocity slowdown of about c/54 with a transmission through the cell of about 15%. This pulse corresponds to a probe Rabi frequency of 0.03 cm^{-1} and a coupling laser Rabi frequency of 0.23 cm^{-1}. The values for the pulse delays are in excellent agreement with theory.

The values of the probe transmission, however, seem to indicate a value for the dephasing rate of the 1-2 channel, Γ_2 , which is almost two orders of magnitude larger than predicted based on a simple nonresonant collisional dephasing model. We have reason to believe that this discrepancy is not due to unaccounted Pb-Pb collisional broadening and are presently investigating other possible sources for this result. The absorption coefficient (for exponential loss) has an experimentally measured inverse square dependence on the coupling laser Rabi frequency, indicating that the effective dephasing mechanism has a Lorentzian profile. Several possibilities for this effective dephasing mechanism are currently under investigation.

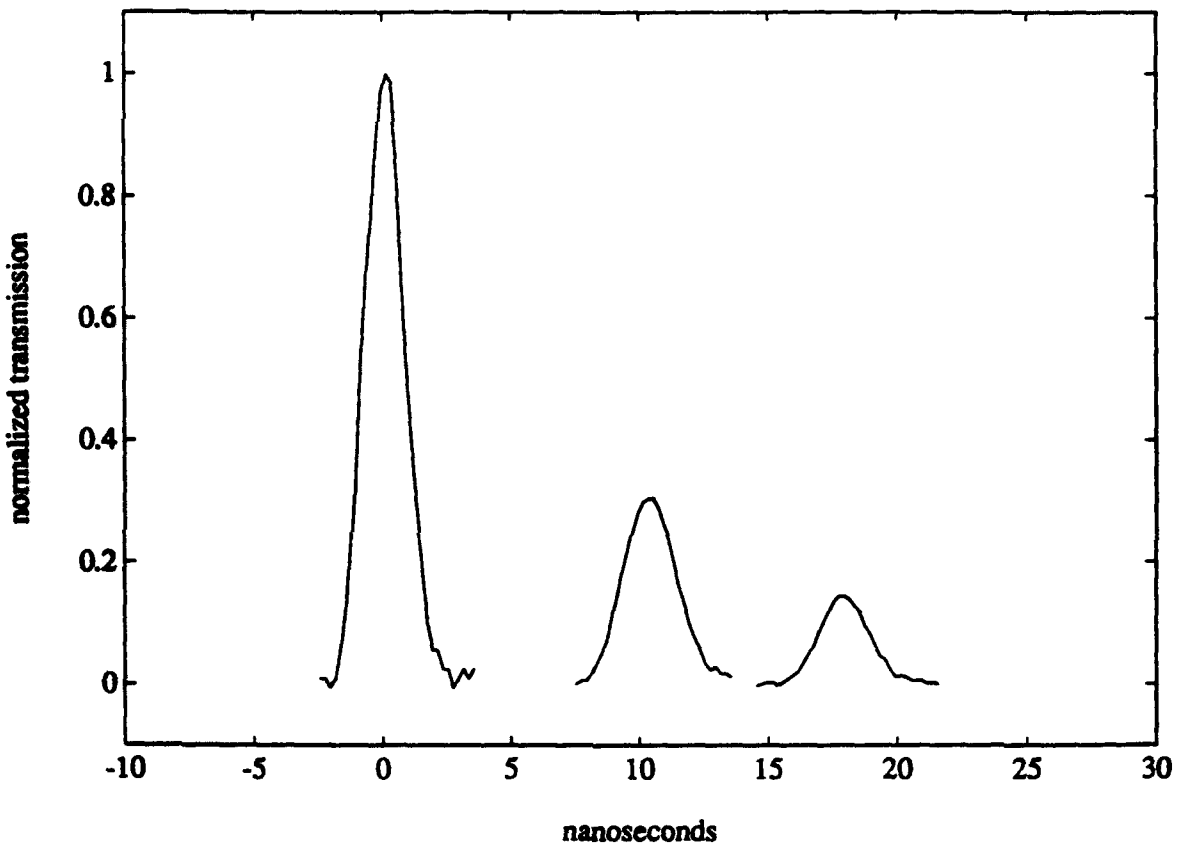

Fig. 2. **Weak-probe pulse propagation in EIT. Unity on the vertical scale indicates the transmission of the probe through the cell when it is far detuned from the resonance line. The output pulses centered at 10 ns and 18 ns are for values of the coupling laser Rabi frequency $\Omega_c = 0.30\ cm^{-1}$ and $\Omega_c = 0.23\ cm^{-1}$, respectively.**

C. LARGE SIGNAL EFFECTS IN ELECTROMAGNETICALLY INDUCED TRANSPARENCY (EIT)

(A. Kasapi and M. Jain)

The dynamics of pulse propagation in EIT become considerably more complex in the large-signal regime. By large signal we mean the regime where the (previously weak) probe Rabi frequency is increased so that it becomes comparable to and even exceeds the coupling laser Rabi frequency. For this set of conditions, we begin to transfer significant fractions of the ground state $|1\rangle$ population into level $|2\rangle$ and back. The coupling laser still has a pulsewidth much larger than the probe laser. As a result, as the probe pulse turns on and then gradually off, population is transferred adiabatically from the ground state to the metastable level $|2\rangle$ and then back, respectively. This produces substancial pulse reshaping effects on both the probe and the coupling laser pulses.

We have observed severe pulse shape distortions due to these effects experimentally. The Pb atomic density was measured to be $N = 1.1 \times 10^{14} / cm^3$ for these experiments. Figure 1 shows an experiment performed using the 2-ns probe pulse and the 100-ns coupling laser pulse. Note that the peak of the probe pulse suffers a delay of 7 ns (group velocity c/21), the output probe pulse is significantly distorted, and is broadened to about twice its input pulsewidth and also shows a sharp falling edge. The coupling laser also acquires a bump on it just as the rising edge of the input probe pulse begins to transfer population to level $|2\rangle$, thereby generating more coupling laser photons. The dip in the coupling laser as these photons are recycled back is not as visible. The Rabi frequency of the probe for this

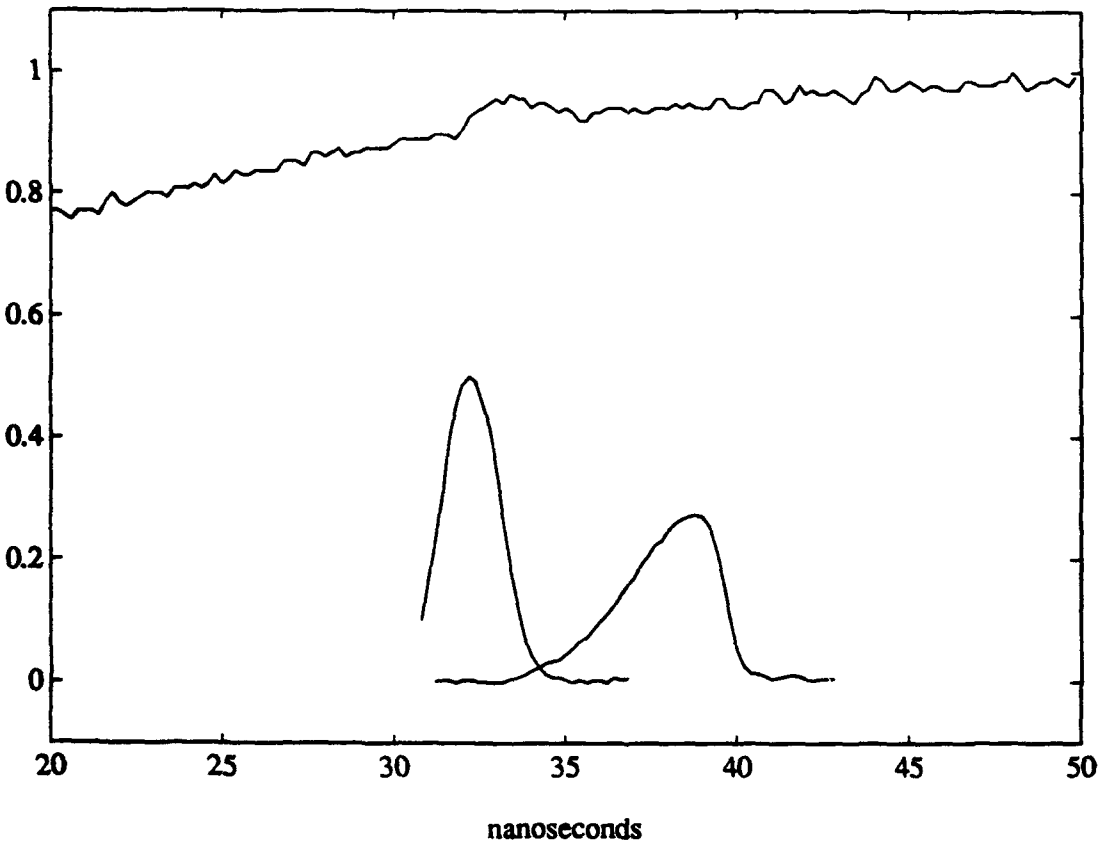

Fig. 1. Large signal propagation in EIT. The probe pulse length is 2 ns, $\Omega_p = 0.6\ cm^{-1}$, and $\Omega_c = 0.4\ cm^{-1}$. The vertical scale is arbitrary.

experiment is about 0.6 cm^{-1} (± 50%) and that at the coupling laser is 0.4 cm^{-1}, so that they are comparable.

We also performed experiments using the full (unshaped) 14 ns probe and the 100-ns coupling laser pulses. Figure 2 shows the results of this work. In this experiment, we used a lower coupling laser Rabi frequency of 0.2 cm^{-1} and increased the probe Rabi frequency to 1.2 cm^{-1}. Further, the longer probe pulse means a seven-fold increase in the available probe energy. The resulting distortions in the coupling laser pulse are startling. The strong probe (intensity 36 times that of the coupling laser) shows only small distortions (the output probe pulse is the smaller of the two) and the rising edge is somewhat steepened, while the falling edge is slower than the input pulse. Also, the output probe pulse is somewhat broadened. The output coupling pulse, however, has spectacular features. We note a sharp bump and dip which looks like a derivative of the input probe pulse, which is as expected from theory and is accounted for by the transfer of population to and back from level $|2\rangle$. There is, however, also a significant dip in the coupling laser output pulse at a delay of 35-40 ns from the input probe pulse. This corresponds to population in level $|2\rangle$ being cycled to level $|3\rangle$ and then, presumably, to level $|1\rangle$. Note that the duration of this dip is on the order of 3 ns, a much narrower feature than the input probe pulses. This feature is observed consistently for this set of experimental conditions, but, as of yet, we have no clear explanation for it.

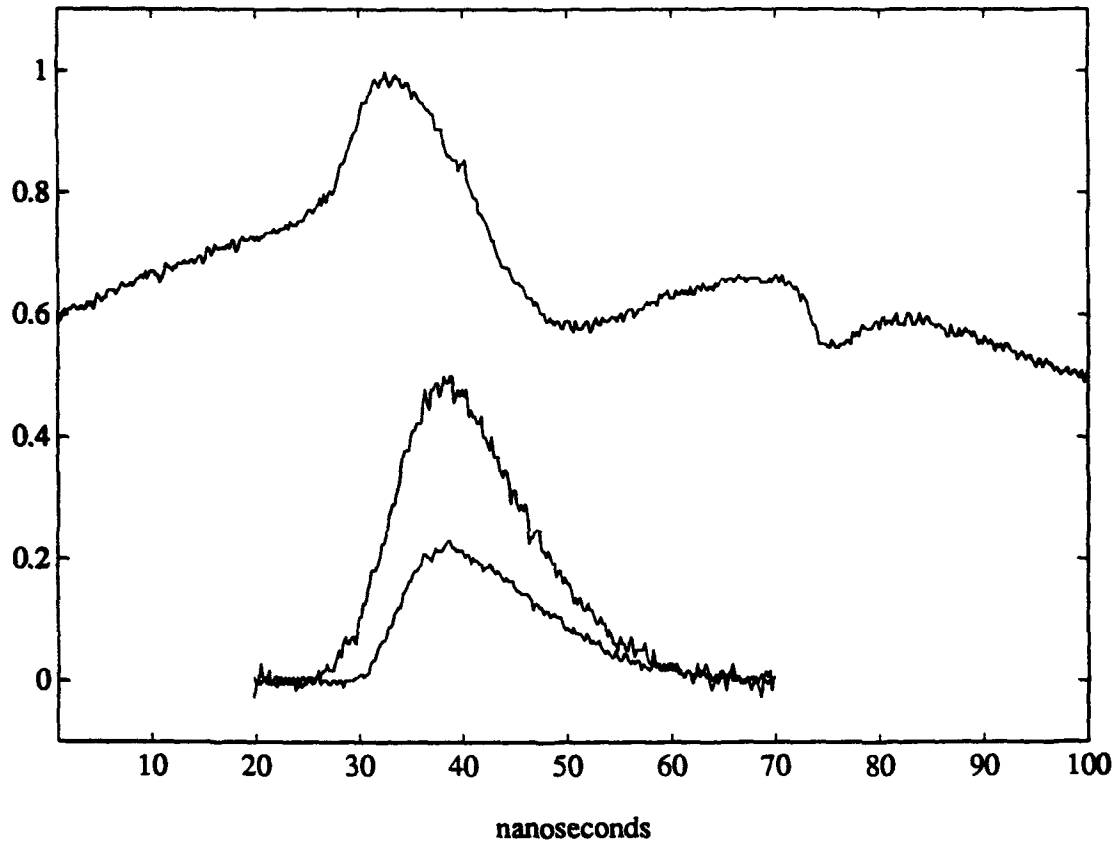

Fig. 2. **Large signal propagation in EIT. The probe pulse length is 14 ns, $\Omega_p = 1.2\,cm^{-1}$, and $\Omega_c = 0.2\,cm^{-1}$. The vertical scale is arbitrary.**

D. EXPERIMENTS IN NONLINEAR OPTICS USING ELECTROMAGNETICALLY INDUCED TRANSPARENCY (EIT)

(M. Jain)

1. INTRODUCTION

In the last three decades there has been very extensive research on nonlinear optical mixing of existing laser frequencies to access portions of the spectrum where lasing action is not easily obtainable. Various techniques have been developed over the years to perform efficient frequency-mixing. Today, sum-frequency generation, as well as parametric oscillation via the second-order nonlinearity in some crystals, allows efficient generation in the region of the spectrum from just under 200 nm in the ultraviolet to about a few microns in the infrared. Generation in the VUV and the mid-to-far-infrared region typically requires four-frequency mixing in atomic vapors. This has traditionally been plagued by poor efficiencies due to the relatively small third-order nonlinear susceptibility as compared to the second-order nonlinearities utilized in crystals. The small third-order susceptibility results from large detunings of the applied fields from the relevant atomic transitions, necessitated by transparency and phasematching requirements. For atomic densities on the order of $10^{16}/\text{cm}^3$, one typically needs to detune the generated radiation by a few wavenumbers to obtain a 10-cm absorption depth, and about 10^3cm^{-1} to obtain a 10-cm coherence length. In the absence of phasematching, which is often difficult, we are forced to generate radiation at large detunings, which leads to typical conversion efficiencies on the order of a few-tenths of a percent with pump intensities in the GW/cm^2 regime. If the media is phasematched, we are limited only by the absorption depth and can generate radiation to within a few wavenumbers of the line.

However, to achieve the largest possible enhancement in $\chi^{(3)}$, we need to generate on-resonance. To accomplish this we need to overcome the Doppler-broadening of the medium and achieve transparency on line center, in addition to being phasematched. It has been shown both theoretically and, more recently, experimentally, that this may be achieved using EIT. This makes it possible, using only moderate pump intensities, to obtain conversion efficiencies in a $\chi^{(3)}$ process which are comparable to those currently obtained using second-order nonlinearities in crystals.

We propose a series of experiments which are intended to fully exploit the vast potential of EIT as it bears on nonlinear optical processes. These are described in detail in the following sections.

2.1. High-Efficiency, Four-Frequency Mixing

Introduction. A little over a year ago, we reported the observation of EIT-related interference effects in a nonlinear optical process. This experiment was the first demonstration of electromagnetically induced phasematching in a four-frequency mixing process and we observed an enhancement in the generated signal of more than a factor of 50. This result was close to that predicted by theory for this experiment and dramatically showed the onset of EIT effects in a nonlinear optical process. The work was, however, limited to relatively small conversion efficiencies due to laser system inadequacies. We now have the high-power laser systems with carefully controlled frequency stability that are key to phasematching nonlinear optical processes using EIT.

With EIT we can perform four-frequency mixing with two of the lasers independently tuned on line-center (Fig. 1). The two resonant lasers (at 283 nm and 406 nm) create a coherent population trapped state, thereby

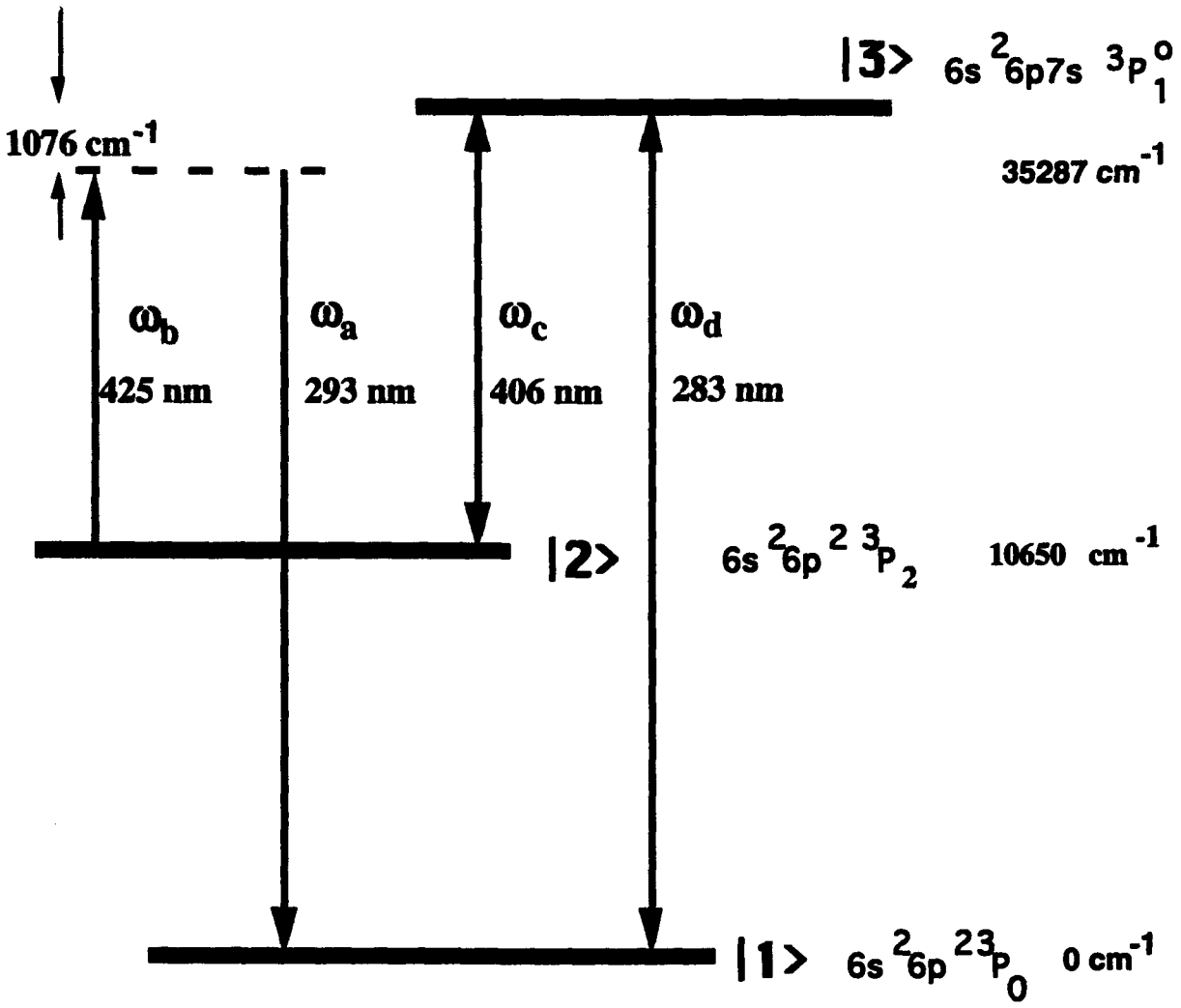

Fig. 1. High-efficiency, four-frequency mixing in Pb vapor.

inducing transparency on line-center. These lasers create a coherent polarization on the $|1\rangle - |2\rangle$ channel which then beats against an additional input laser frequency (in this case, at 425 nm) to efficiently generate the four-frequency mixing signal at 293 nm. In this experiment we will further utilize the coherence (narrow linewidth) of the lasers to phasematch the process by small, controlled detunings of the resonant lasers.

Experiment. The proposed experiment is in Pb vapor with levels $|1\rangle$ and $|2\rangle$ being the $6s^2 6p^2\,(J=0)$ and $(J=2)$ states of the ground manifold, respectively. Level $|3\rangle$ is the $6s^2 6p7s\,(J=1)$ level of atomic Pb (Fig. 1). We apply frequency-stabilized lasers on the $|1\rangle - |3\rangle$ and $|2\rangle - |3\rangle$ transitions at 283 nm and 406 nm, respectively. We will choose a ratio of Rabi frequencies at 406 nm to that at 283 nm of $\Omega_c / \Omega_p = 3$; this yields a ratio of trapped population in level $|2\rangle$ to that in the ground state of 1:9. We also apply an arbitrary pulse of light at 425 nm (obtained from the doubled 850-nm Ti:Sapphire laser). This laser is at a detuning of over a thousand wavenumbers from level $|3\rangle$ and generates a matched pulse at 293 nm, as predicted by the theory of electromagnetically induced transparency with matched pulses.

Conversion Efficiency. The expected conversion efficiency from 425 nm to 293 nm for this process is about 40% with a cell length of 22 cm and a cell density of $3\times10^{15}/\mathrm{cm}^3$. The intensities we require for the resonant laser pulses at 406 nm and 283 nm are on the order of 10 $\mathrm{MW/cm}^2$. Since the intensities of all the pump lasers are comparable in this experiment, we expect absolute conversion efficiencies (generated power density at 293 nm over total input power density) in the vicinity of 10%. Note that these calculations are all in the rotating-wave approximation and ignore pump depletion. There is also a competing process where the 425 nm laser beats

against the $|1\rangle\langle 2|$ dipole moment to generate a difference signal at 775 nm. However, the absolute conversion efficiency for this process is estimated to be less than 0.5%.

Phasematching and Pulse Modulation. This experiment will utilize (and critically depend on) the narrow linewidths of the two lasers at 406 nm and 283 nm. To ensure phasematched generation we will need to control the absolute frequencies of the two lasers to within a few MHz. This requirement comes from the steep slope of the real part of the linear susceptibility near resonance in EIT. This slope varies as the inverse of the sum of the squares of the Rabi frequencies of the two lasers. Therefore, the requirement on the laser frequency stability is somewhat relaxed by choosing larger Rabi frequencies. In any case, with the current laser systems, we will need a frequency stability of about 30 MHz, even if we use a large Rabi frequency of about $4-5\,\mathrm{cm}^{-1}$ on the coupling laser at 406 nm. At a Rabi frequency of $5\,\mathrm{cm}^{-1}$, the slope of the real linear susceptibility produces a 2-ns delay for the 283-nm laser for our 10-cm cell length. This group-velocity slip is small compared to the pulse lengths.

Note that the radiation at 425 nm could be broadband (for instance, have information impressed on it by frequency modulation) and the modulation will be replicated on the generated signal at 293 nm since its envelope spectrum will match that of the 425-nm laser. This can be a useful method of transferring modulation from a pump laser to a generated four-frequency mixing signal.

2. 2 Efficient VUV Generation

Introduction. Ladder systems in rare gases are especially well suited to VUV generation. Krypton has the desirable property that the energy levels are such that we may use convenient Ti:Sapphire laser frequencies for the pump lasers. The generated wavelength is 124 nm in the VUV, for which LiF windows are available; hence, a cell with a few torr of Kr gas is readily constructed. Also, this ladder system behaves like a true three-level system. As shown in Fig. 2., levels $|1\rangle$ and $|2\rangle$ have the same $J = 0$ and, therefore, couple similarly to level $|3\rangle$. This situation is ideal for EIT. Therefore, in addition to using this system for VUV generation, we will utilize it as a prototype for studying large-signal EIT in ladder systems, which promises some very interesting results.

Experimental Details and Conversion Efficiency. The four-frequency mixing scheme in this system is shown in Fig. 2. The two-photon pump from level $|1\rangle$ to level $|2\rangle$ is a 848-nm Ti:Sapphire laser which is frequency quadrupled to 212 nm using two BBO doubling crystals. This requires only minor changes in the 850-nm system we currently have in operation. The coupling laser will be another Ti:Sapphire laser at 760 nm, which is close to the gain peak of Ti:Sapphire and diode lasers are readily available at this frequency. With some effort we should readily be able to modify the 812-nm system currently available to produce an output at 760 nm.

As mentioned earlier, this ladder system in Kr behaves like a true three-level system. Level $|2\rangle$ couples strongly only to level $|3\rangle$ below. Level $|2\rangle$ couples very weakly to another level $5s'^{\,o}$ $(J = 1)$ (at 85848 cm^{-1}) with an oscillator-strength-degeneracy product $gf = 0.0002$; this level $[5s'^{\,o}\ (J = 1)]$ couples to the ground level $|1\rangle$ with $gf = 0.3$ and has a natural lifetime of 2.1 ns. Hence, there is not the possibility of level $|2\rangle$

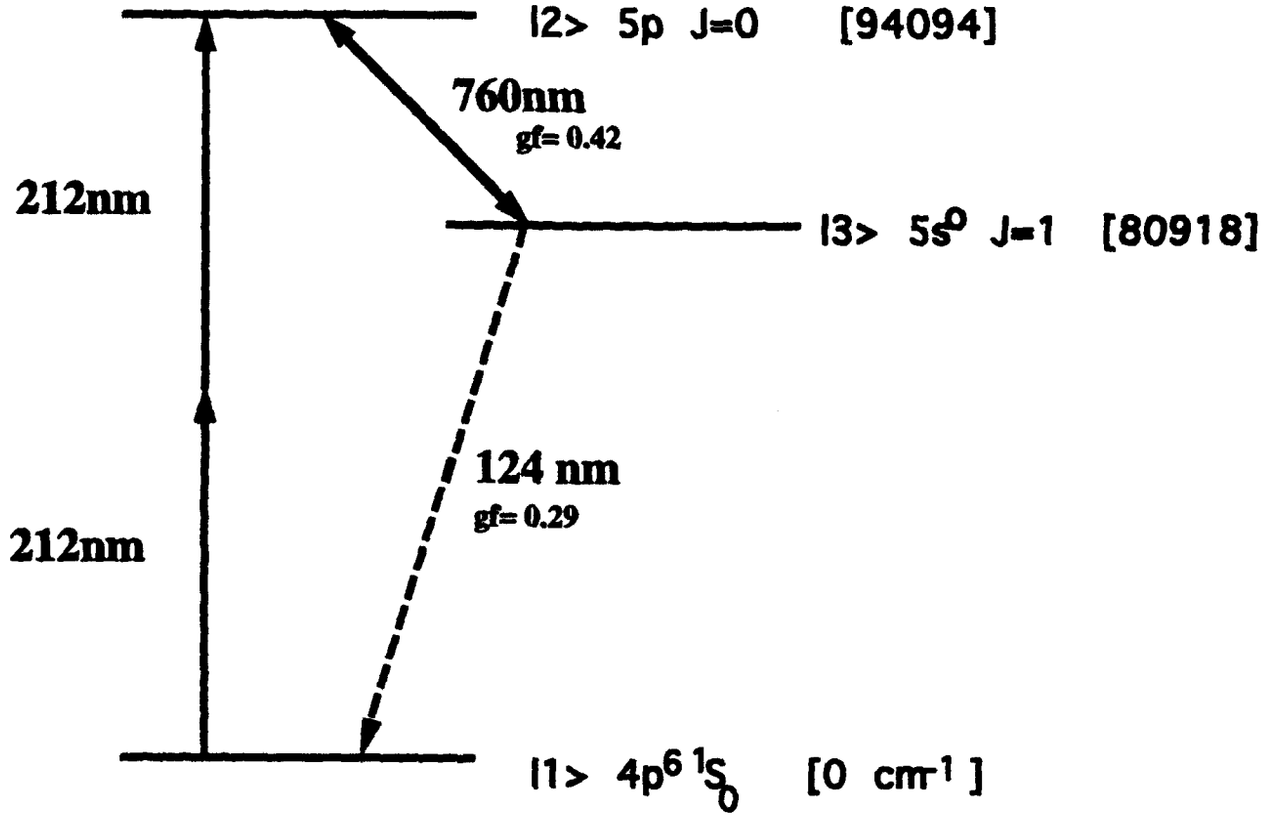

Fig. 2. Energy level diagram of the Kr ladder system for VUV generation.

coupling strongly to some level below which is not strongly coupled to ground. If this were possible, the "trapped" population in level $|2\rangle$ would quickly relax to this lower level. This situation is to be avoided when working with ladder systems.

We estimate the conversion efficiency for VUV generation as follows: The $|2\rangle - |3\rangle$ transition has a $gf = 0.42$ and a matrix element of $\mu_{23} = 1.9$ a.u. For the $|1\rangle - |3\rangle$ transition we have $gf = 0.29$ and $\mu_{13} = 0.63$ a.u. Level $|2\rangle$ has a natural lifetime of 20.8 ns (7.6 MHz linewidth) and level $|3\rangle$ has a natural lifetime of 2.4 ns (66 MHz linewidth). We have not yet calculated the effect of collisional broadening, which will probably dominate the homogeneous linewidth for level $|3\rangle$, since it is resonantly broadened by ground state atoms. The two-photon inhomogeneous (Doppler) FWHM linewidth for this system is about $0.13\ \text{cm}^{-1}$ at room temperature. For a cell density of $10^{16}/\text{cm}^3$, a cell length of 20 cm, and laser intensities of $I(760\ \text{nm}) = 1\ \text{MW/cm}^2$ (about $2.2\ \text{cm}^{-1}$ Rabi frequency); $I(212\ \text{nm}) = 200\ \text{kW/cm}^2$, we have a small signal net conversion efficiency of about 1% to 124 nm. Note that we are predicting this 1% conversion efficiency for pump lasers with intensities in the $1\ \text{MW/cm}^2$ or less regime and with a $\chi^{(3)}$ with one large denominator for the detuning from level $|3\rangle$ of the two-photon pump to level $|2\rangle$. This shows the potential of EIT when applied to frequency-mixing processes.

Possible Difficulties. There are, however, some possible problems to be aware of when working with ladder systems, resulting from the fact that in EIT we create a trapped population in level $|2\rangle$ and, also, level $|3\rangle$ below is kept nearly empty. The 212-nm lasers will photoionize level $|2\rangle$ and cause a rate out of that level. If we take $10^{-17}/\text{cm}^2$ as the photoionization cross section, this gives a rate of $10^7/\text{s}$ at $1\ \text{MW/cm}^2$ of laser power, which is

significant, but not problematic. The 760-nm laser will carry level $|2\rangle$ to 107269.8 cm^{-1}, which is 335 cm^{-1} away from the closest line [6d (J = 0)] . This will cause a time-varying ac stark shift of level $|2\rangle$ which is dependent on the 760 nm intensity. At 1 MW/cm^2, however, this effect will be small and not significantly affect the phasematched generation of the VUV radiation.

Amplified spontaneous emission from level $|2\rangle$ to level $|3\rangle$ will be suppressed in the forward direction (matched pulse theory), but will be present in the backward direction and cause and additional rate out of level $|2\rangle$. The gain cross section will depend on the population in level $|2\rangle$. Hence, this effect seems like an ultimate limitation to large conversion efficiencies to 124 nm. How large a conversion efficiency we can obtain before this effect causes real damage requires experimental work. The Kr system is excellent for studying the possible limitations of large-signal EIT behavior in ladder systems.

2. 3 Mid-To-Far-Infrared Generation

Introduction. An experiment which generates radiation in the mid-to-far-infrared can also be performed in the same Pb vapor system as that used in Section 2.1 for high-efficiency, four-frequency mixing. Again, we apply two resonant lasers (at 283 nm and 406 nm) which create the coherent population trapped state and induce transparency on line-center. As shown in Fig. 3, we now mix a laser at 850 nm with the coherent polarization on the $|1\rangle - |2\rangle$ channel to generate light at 9 μm in the infrared. Here, the conversion efficiencies will be smaller since we are operating at a large detuning. By tuning the 850-nm Ti:Sapphire laser in the region of 700 nm to 925 nm, we

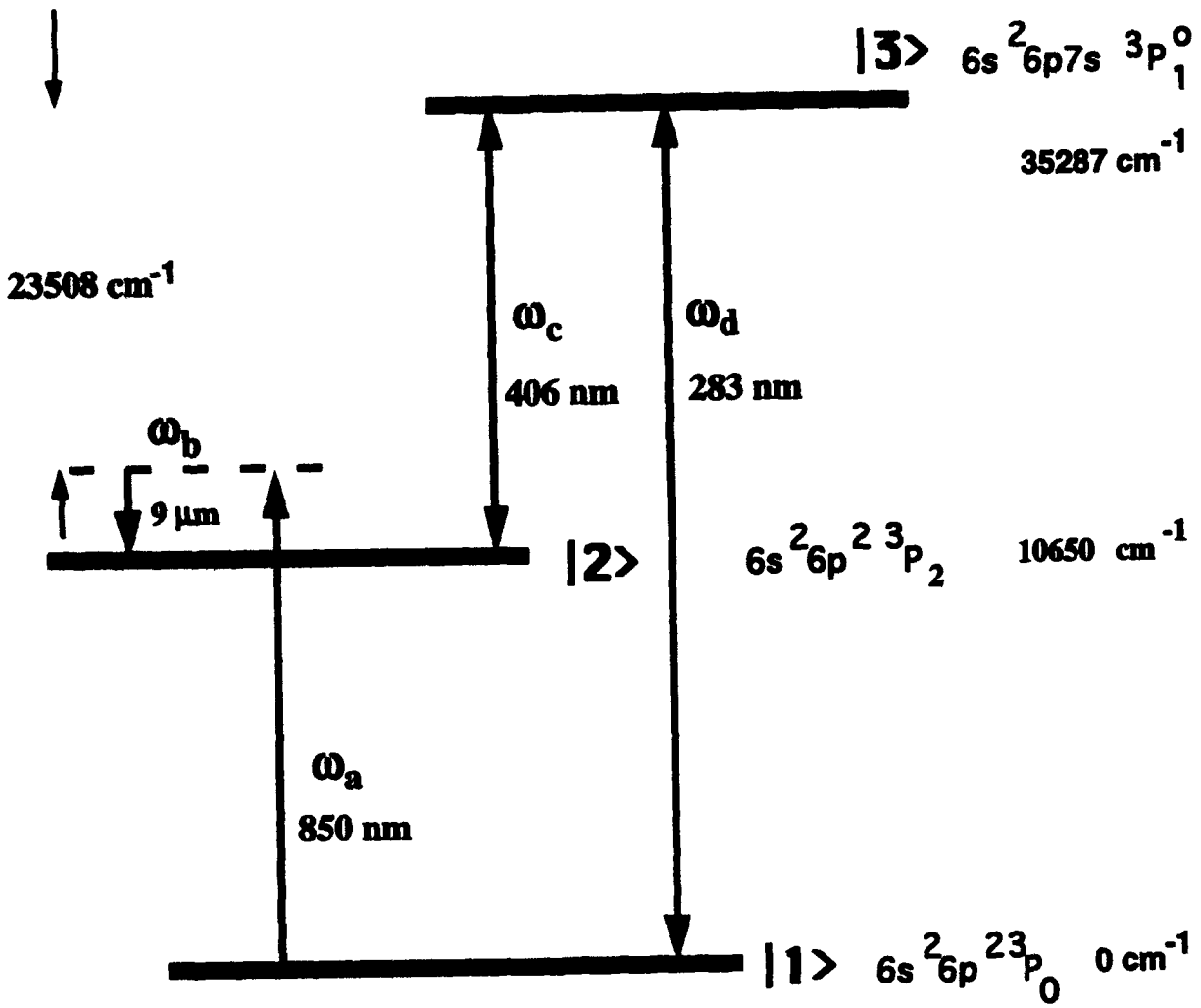

Fig. 3. Mid-to-far-infrared generation in Pb vapor.

can generate correspondingly in the infrared from 2.75 μm to 62 μm with conversion efficiencies in the few-tenths of a percent region.

Experiment. We again apply frequency-stabilized lasers on the $|1\rangle - |3\rangle$ and $|2\rangle - |3\rangle$ transitions at 283 nm and 406 nm, respectively. The 850-nm radiation is at a detuning of about 23500 cm^{-1} from level $|3\rangle$ and generates radiation at 9 μm in the infrared. Note that the 850-nm light is the fundamental frequency of the Ti:Sapphire system which is tripled to 283 nm. Hence, we can perform this experiment with the two currently existing laser systems. For a cell length of 22 cm and an atomic density of $9 \times 10^{15} / cm^3$, we predict a conversion efficiency of about 1% to the infrared. In calculating this value we have assumed the ratio of Rabi frequencies of the 406 nm to the 283 nm lasers to be 3:1. For this system, we also have a competing process with about a 3% conversion efficiency, where the 850-nm laser mixes with the $|1\rangle\langle 2|$ coherent polarization and sums to generate 446-nm radiation. These calculations are all in the rotating-wave approximation. To the extent that we can tune and modulate the light at 850 nm, these characteristics will be replicated on the 9 μm radiation. This provides a useful method of producing modulated outputs in regions of the infrared where direct modulation is either difficult or unfeasible. As mentioned above, we can utilize the broad tuning range of Ti:Sapphire to generate in the infrared from 2.7 μm to, in principle, dc, with absolute conversion efficiencies in the few-tenths of a percent regime (limited, of course, by the photon-to-photon conversion efficiency for the long wavelengths).

E. STUDIES OF LASERS WITHOUT INVERSION (LWI)

(A. Merriam)

1. INTRODUCTION

It has been shown recently [1] that the traditional criterion for lasing, namely that the population of the upper lasing level N_2 be larger than that of the lower level N_1, is not a requirement for obtaining laser amplification. It is a necessary condition for systems with no atomic coherence. For such systems, transparency to the emitted photons, and hence net gain, is possible only when $N_2 > N_1$. For systems with atomic coherence, on the other hand, a destructive interference may be selectively introduced into the absorption profile of lower-level atoms, but not into the emission profile of upper-level atoms. The system thus displays nonreciprocal gain and loss profiles and may provide gain when an inversion condition does not exist.

The importance and potential benefit of Amplification and Lasing Without Inversion (AWI and LWI, respectively) becomes apparent when one considers the difficulties in realizing an x-ray or even UV laser; inversion of the atomic basis becomes more and more difficult because the lifetime of a state quickly decreases with increasing energy. It is our aim to construct and demonstrate the usefulness of a quantum-interference-based inversionless optical amplifier.

2. ABSORPTION AND EMISSION PROFILES

Our prototype three-level atomic system is shown in Fig. 1. We consider the behavior of such a system under the influence of two coherent cw fields. The coupling field couples states $|2\rangle$ and $|3\rangle$, while the probe field

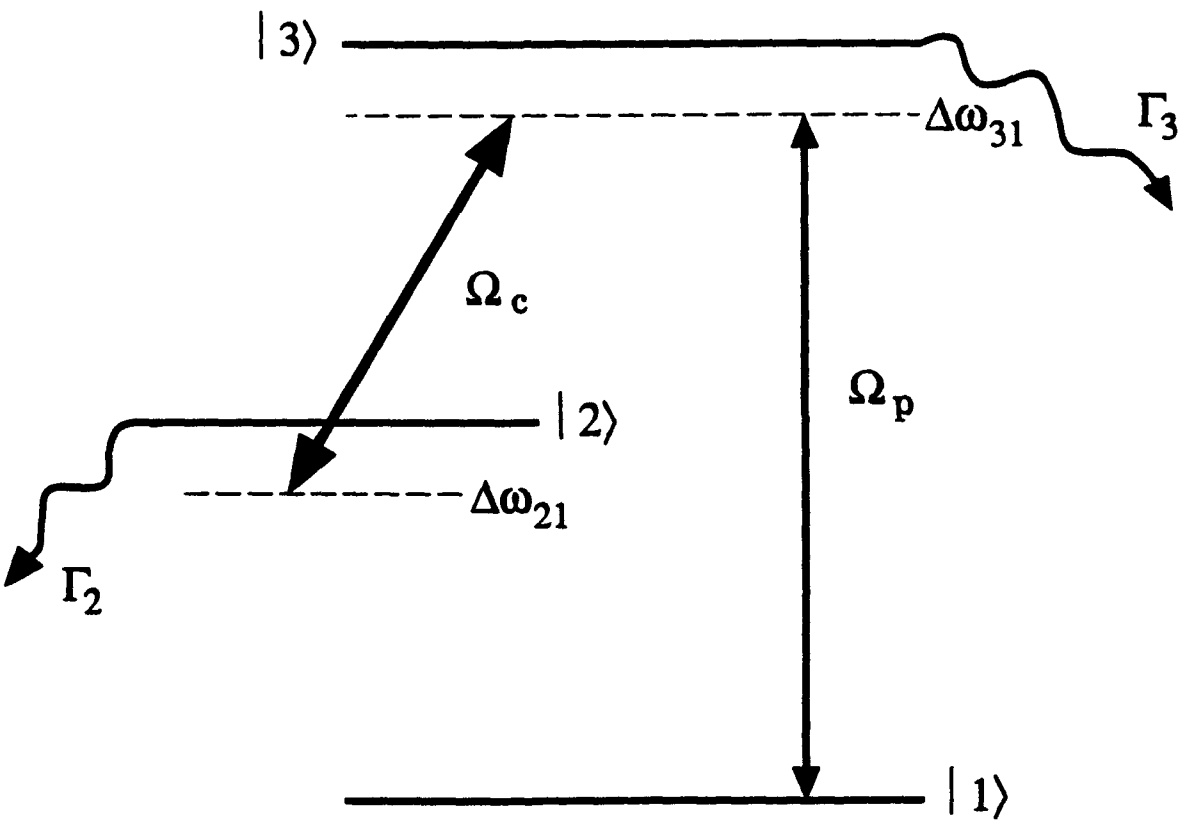

Fig. 1. Prototype three-level system.

couples states $|1\rangle$ and $|3\rangle$ (and no others), as shown. We have demonstrated that a remarkable cancellation of absorption can be realized in such a system. This effect is known as Electromagnetically Induced Transparency (EIT), the rendering of a previously opaque atomic transition transparent. With a metastable state $|2\rangle$, the resulting absorption profiles are like that shown in Fig. 2, where the dashed curve indicates the usual absorption profile of the atomic system without the coupling field applied. The zero at line center is not simply the sum of the reduced absorption tails of the Rabi-split levels, but is a perfect cancellation resulting from a destructive quantum interference. The application of the coupling field renders the system transparent and hence lossless; but, if nothing further is done, the system will remain gainless as well. By selectively pumping the transparent system, however, we observe a gain cross section that is on the order of the absorption cross section of the bare $|1\rangle - |3\rangle$ transition.

In order to fully describe the absorption and emission characteristics of the atomic system, we must consider three atomic initial conditions, corresponding to whether an individual atom at $t = 0$ is in state $|1\rangle$, $|2\rangle$, or $|3\rangle$ (*n.b.* the "pumping" of a state can be thought of as the random excitation of these initial conditions). We begin by examining numerical solutions of the coupled differential equations, which offer intuitive explanations of the system's behavior. The parameters of the simulations are chosen so that the system is transparent on line center. Figure 3(a) shows the probability for level $|1\rangle$ occupation, $|b_1(t)|^2$, for the case that the atom is originally in state $|1\rangle$. In general, if a probe field is applied to a two-level atom, the absorption profile will consist of a non-cancellable transient term (Δ) and a non-zero steady-state golden-rule (W_{ab}) term. For the three-level atom and zero detunings, however, the steady-state term is zero due to the transparency

effect, and the absorption consists solely of the transient term. This process, by which a fraction of the state $|1\rangle$ atom leaves state $|1\rangle$, is, of course, accomplished at the expense of the probe field; the energy loss is proportional to the fraction of atomic population that is removed. Some of this population goes into state $|2\rangle$, and some (for cw fields, *twice* as much as goes to state $|2\rangle$) is lost through state $|3\rangle$. Physically, the fraction of the atom that is transferred to state $|2\rangle$ is that required for the atom to become transparent to the probe frequency. (The transient loss is a result of the cw fields which were applied, and is not cancellable; a transient absorption of zero may be obtained if the probe field is brought up "adiabatically," i.e., slowly compared to the quadrature sum of the Rabi frequencies.) After the atom has been "prepared" in this transparent state, it contributes no further absorption to the problem and may be ignored.

What happens if we instead put an atom into state $|2\rangle$ or $|3\rangle$? Now, the salient quantity is the fraction of probability, or equivalently, population, that is transferred to state $|1\rangle$ at times large compared to the transient. In general, the atom in states $|2\rangle$ or $|3\rangle$ (which are strongly coupled by the strong coupling field), will decay quickly via the lifetime of state $|3\rangle$. As these levels decay, however, they drive the growth of the state $|1\rangle$ population. This behavior may be observed in Figs. 3(b) and 3(c). Note that the fraction of population transferred to state $|1\rangle$ for the case when the atom is initially in state $|3\rangle$ is zero for zero detunings. The gain obtained from an atom initially in state $|2\rangle$ or $|3\rangle$ is equal to the fraction of population that is moved to state $|1\rangle$ at long times. Note that, since the transparent atoms can no longer absorb the probe radiation, amplification in the atomic system can occur even under conditions where the lower-level population is arbitrarily large!

3. ANALYTIC SOLUTIONS

The coupled atomic coefficient equations may also be solved analytically, *in the limit of small probe Rabi frequency*, with the following results. An atom which is initally in state $|1\rangle$ has a probability P_{ab} of being absorbed, where, as mentioned earlier, P_{ab} is the sum of a transient and a steady-state term: $P_{ab} = \Delta + W_{ab}t$, where

$$W_{ab} = |\Omega_p|^2 \frac{\Gamma_2\left(|\Omega_c|^2 + \Gamma_2\Gamma_3\right) + 4\Gamma_3\Delta\omega_{21}^2}{\left(4\Delta\omega_{21}\Delta\omega_{31} - \Gamma_2\Gamma_3 - |\Omega_c|^2\right)^2 + 4\left(\Gamma_2\Delta\omega_{31} + \Gamma_3\Delta\omega_{21}\right)^2}$$

and for metastable state $|2\rangle$,

$$\Delta = 8|\Omega_p|^2 \frac{\left(\frac{|\Omega_c|^2}{4} + \Delta\omega_{21}^2\right)\left[\left(4\Delta\omega_{21}\Delta\omega_{31} - |\Omega_c|^2\right)^2 - 4\Gamma_3^2\Delta\omega_{21}^2\right]}{\left[\left(4\Delta\omega_{21}\Delta\omega_{31} - |\Omega_c|^2\right)^2 + 4\Gamma_3^2\Delta\omega_{21}^2\right]^2}$$

In these equations, Ω_c and Ω_p are the coupling and probe Rabi frequencies, Γ_2 and Γ_3 are the lifetimes of the bare states $|2\rangle$ and $|3\rangle$, and $\Delta\omega$ are the detunings as shown in Fig. 1. Note that the golden-rule absorption rate is functionally identical to the imaginary part of the complex linear susceptibility as derived in Ref. 2; in fact, W_{ab} has all EIT effects contained within it.

Similarly, the probability G_2 that an atom, at times long compared to the transient, makes a transition to state $|1\rangle$ after starting in state $|2\rangle$ is

$$G_2 = \frac{|\Omega_p|^2 |\Omega_c|^2}{\left(4\Delta\omega_{21}\Delta\omega_{31} - \Gamma_2\Gamma_3 - |\Omega_c|^2\right)^2 + 4(\Gamma_2\Delta\omega_{31} + \Gamma_3\Delta\omega_{21})^2}$$

and the probability G_3 that the atom makes a transition to state $|1\rangle$ after starting in state $|3\rangle$ is

$$G_3 = \frac{4|\Omega_p|^2 \left(\Delta\omega_{21}^2 + \frac{\Gamma_2^2}{4}\right)}{\left(4\Delta\omega_{21}\Delta\omega_{31} - \Gamma_2\Gamma_3 - |\Omega_c|^2\right)^2 + 4(\Gamma_2\Delta\omega_{31} + \Gamma_3\Delta\omega_{21})^2}$$

A plot of the absorption rate, W_{ab} , and emission probability, G_2 , normalized to the transition rate of the uncoupled $|1\rangle - |3\rangle$ system for a three-level atom, is shown in Fig. 4, as a function of normalized probe-field detuning. For this curve, $\Omega_c = 0.5\,\Gamma_3 = 0.1$. Note that the profiles are non-reciprocal for the coupled three-level atom, which means that at line center we may expect significant net gain.

4. GAIN AND LOSS

The equations of the last section may be used to determine the overall gain and loss in the atomic system. The energy gain at the probe frequency, due to the competing emission and absorption processes, is simply

$$dE(\omega_p) = \left[R_2 G_2 + R_3 G_3 - (W_{ab} N_1 + R_1 \Delta)\right] \hbar\omega_p$$

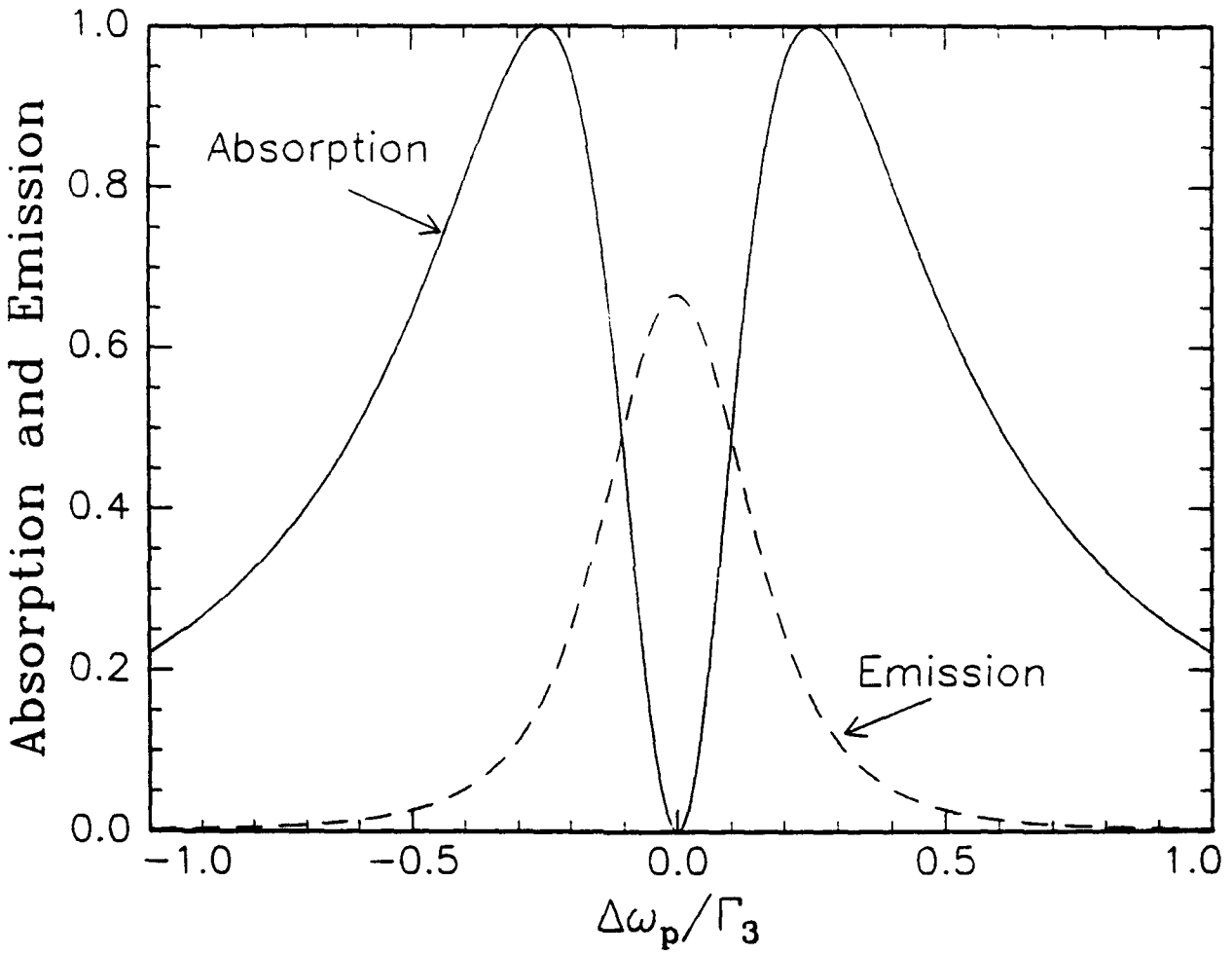

Fig. 4. Nonreciprocal absorption and emission profile of coupled three-level atom as function of normalized detuning.

where R_i is the rate into level $|i\rangle$ and N_i is the population of state $|i\rangle$. As a specific example, consider a transparent system, where $W_{ab} = 0$, and with a metastable state $|2\rangle$. Then, the losses are solely due to the pumping of state $|1\rangle$ atoms and the above formula indicates that gain is achieved *if the pumping rate of state $|2\rangle$ atoms is at least twice that of state $|1\rangle$ atoms.*

The rate formulation is very handy when considering possible experimental systems to demonstrate LWI, but it is important also to show that this gain occurs without inversion; therefore, the above equation is cast into a form which explicitly details the dependence on the atomic populations. We first note that $G_3 << G_2$ for large coupling laser fields. Then, neglecting the rate into state $|1\rangle$ (which includes dephasings of the $|1\rangle - |2\rangle$ channel) and hence avoiding the transient losses, we may write the gain coefficient for metastable state $|2\rangle$ and zero coupling laser detuning as

$$\gamma(\omega_p) = \frac{\sigma(\omega_p)\Gamma_3^2}{\left(4\Delta\omega_{31}^2 - |\Omega_c|^2\right)^2 + 4(\Gamma_3\Delta\omega_{31})^2}\left[\frac{|\Omega_c|^4(N_2+N_3)}{\Gamma_3^2 + 2|\Omega_c|^2} - 4\Delta\omega_{31}^2 N_1\right]$$

where the normalized cross section $\sigma(\omega_p)$ is given by

$$\sigma(\omega_p) = \frac{2\omega_p}{\hbar}\sqrt{\frac{\mu_0}{\varepsilon_0\varepsilon(\omega_p)}}\frac{|\mu_{13}|^2}{\Gamma_3}$$

These equations clearly indicate that for a certain range of probe detunings, net gain is possible even when $N_2 + N_3 << N_1$! This behavior can be verified by re-appraising Fig. 4. Note that the gain of the system goes down as the *square* of the coupler Rabi frequency. In general, to enable transparency, a coupler Rabi frequency must be applied that is at least as

great as the total linewidth of the state under consideration, including collisional and doppler effects. This means that we shall seek to minimize these linewidths in our chosen atomic system.

5. CURRENT RESEARCH

Our aim is to achieve lasers without inversion; the first step is to demonstrate the feasibility of inversionless amplification. To that end we are considering a number of atomic systems to determine which has the best chance of succeeding. A prototype AWI system is shown in Fig. 5; pumping is nominally from state $|1\rangle$ to some higher state $|4\rangle$, which then spontaneously decays into states $|1\rangle$, $|2\rangle$, and $|3\rangle$ and provides the rates R_1, R_2, and R_3 that drive the gain. Some of the parameters upon which we base our decision are:

- Wavelengths easily accessible using current laser systems.
- Minimal Doppler widths, so that the coupler Rabi frequency can be minimized.
- Maximum rates into state $|2\rangle$ relative to state $|1\rangle$.
- Clear indication of amplification without inversion.

The experimental setup can be used in some cases to compensate for difficulties in the particular system if that system is particularly desirable. For example, atomic ladder systems can be run virtually Doppler-free by counter-propagating the probe and coupling lasers. Such is the case in gaseous rubidium. Also, in some cases, levels near level $|1\rangle$, whose parity is the same as level $|1\rangle$, are thermally populated (as is the case, for example, in the LS split ground states $^3P_{0,1,2}$ of lead) and can be pumped into an upper level which cannot decay immediately to state $|1\rangle$ (due to dipole selection rules), leading to much higher pumping efficiencies into state $|2\rangle$.

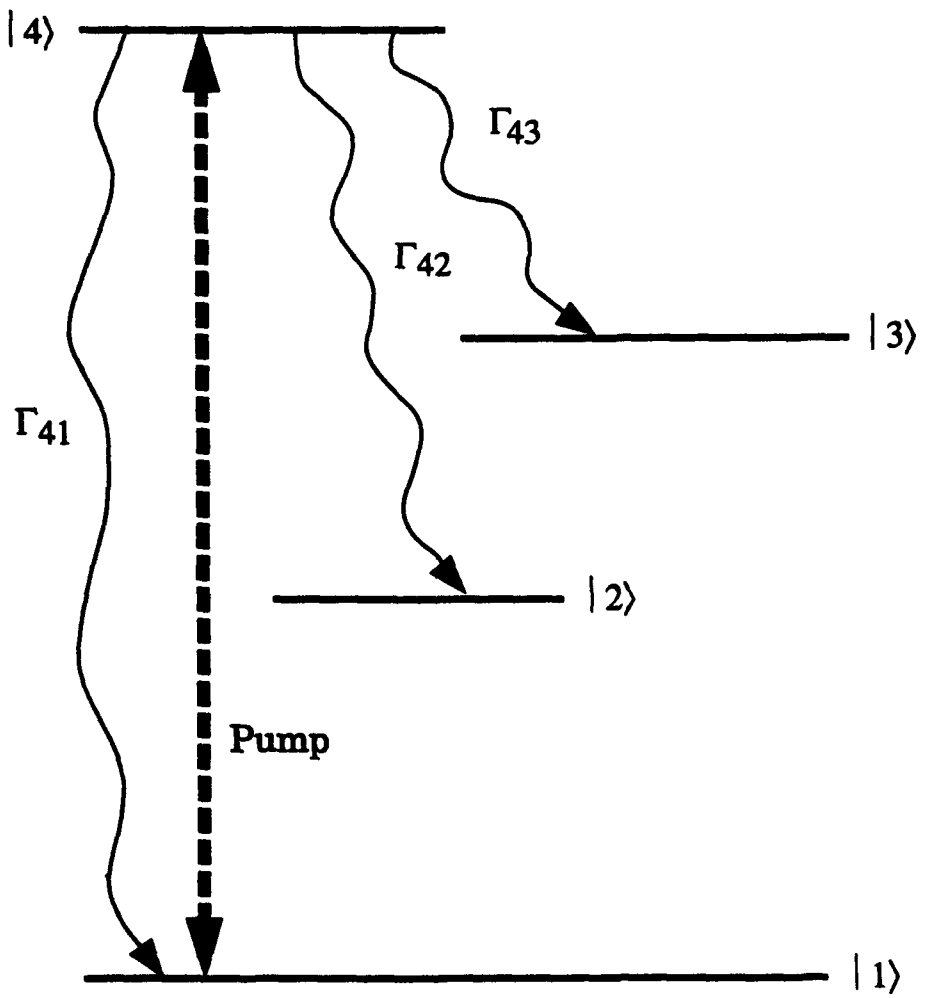

Fig. 5. Prototype of AWI system.

In conclusion, the theoretical basis for lasing without inversion has been described. The conditions for successful demonstration of this effect are such that the particular atomic system must be chosen with care. Current research focuses on the selection and numerical modeling of a suitable atomic system, leading to the design and fabrication of an experiment to demonstrate AWI and LWI.

References

1. S. E. Harris and J. J. Macklin, "Lasers Without Inversion: Interference of Lifetime-Broadened Resonances," *Phys. Rev. Lett.* **62**, 1033 (1989)

2. S. E. Harris, J. E. Field, and A. Imamoglu, "Nonlinear Optical Processes Using Electromagnetically Induced Transparency," *Phys. Rev. Lett.* **64**, 1107 (1990).

PUBLICATIONS

Publications (10/1/91 through 9/30/92)

1. J. E. Field, K. H. Hahn, and S. E. Harris, "Observation of Electromagnetically Induced Transparency in Collisionally Broadened Lead Vapor," *Phys. Rev. Lett.* **67**, 3062-3065 (November 1991).

2. M. H. Sher and S. J. Benerofe, "Prepulsing of Laser-Produced Plasmas for More Efficient Pumping of Extreme-Ultraviolet Lasers," *J. Opt. Soc. Am. B* **8**, 2437-2441 (December 1991).

3. K.-J. Boller, A. Imamoglu, and S. E. Harris, "Electromagnetically Induced Transparency in Sr Vapor," in *Laser Spectroscopy*, edited by M. Ducloy, E. Giacobino, and G. Camy (New Jersey, World Scientific, 1992), pp. 295-300.

4. S. E. Harris, J. E. Field, and A. Kasapi, "Dispersive Properties of Electromagnetically Induced Transparency," *Phys. Rev. A* **46**, R29-R32 (July 1992).

Publications (10/1/92 through 9/30/93)

1. C. P. J. Barty, G. Y. Yin, J. E. Field, D. A. King, K. H. Hahn, J. F. Young, and S. E. Harris, "Studies of a 96.9-nm Laser in Neutral Cesium," *Phys. Rev. A* **46**, 4286-4296 (October 1992).

2. S. J. Benerofe, G. Y. Yin, and S. E. Harris, "116 nm H_2 Laser Pumped by a Traveling-Wave Photoionization Electron Source," in *Vacuum Ultraviolet Radiation Physics*, edited by F. J. Wuilleumier, Y. Petroff, and I. Nenner (New Jersey, World Scientific, 1993), pp. 85-95.

3. C. P. J. Barty, C. L. Gordon III, J. D. Kmetec, B. E. Lemoff, and S. E. Harris, "Ultrashort High Peak Power Lasers and Generation of Hard Incoherent X-Rays," in *Proceedings of of the International Conference on Lasers '92*, edited by C. P. Wang (McLean, VA, STS Press, 1993), pp. 44-51.

4. C. P. J. Barty, B. E. Lemoff, and C. L. Gordon III, "Generation, Measurement, and Amplification of 20-fs High-Peak-Power Pulses from a Regeneratively Initiated Self-Mode-Locked Ti:Sapphire Laser," in *SPIE Proceedings on Ultrafast Pulse Generation and Spectroscopy*, (Bellingham, WA, Society of Photo-Optical Instrumentation Engineers, 1993), 1861, pp. 6-30.

5. B. E. Lemoff, C. L. Gordon III, and C. P. J. Barty, "Design of a Quintic-Phase-Limited Amplification System for Production of Multi-Terawatt 20-fs, 800-nm Pulses," in *OSA Proceedings on Shortwavelength V: Physics with Intense Laser Pulses*, edited by Paul B. Corkum and Michael D. Perry (Washington, DC, Optical Society of America, 1993), pp. 31-35.

6. B. E. Lemoff and C. P. J. Barty, "Cubic-Phase-Free-Dispersion Compensation in Solid-State Ultrashort-Pulse Lasers," *Opt. Lett.* **18**, 57-59 (January 1993).

7. S. E. Harris, "Electromagnetically Induced Transparency with Matched Pulses," *Phys. Rev. Lett.* **70**, 552-555 (February 1993).

8. Maneesh Jain, G. Y. Yin, J. E. Field, and S. E. Harris, "Observation of Electromagnetically Induced Phasematching," *Opt. Lett.* **18**, 998-1000 (June 1993).

9. J. E. Field, "Vacuum-Rabi-Splitting-Induced Transparency," *Phys. Rev. A* **47**, 5064-5067 (June 1993).

10. S. E. Harris, J. J. Macklin, and T. W. Hänsch, "Atomic Scale Temporal Structure Inherent to High-Order Harmonic Generation," *Opt. Commun.* **100**, 487-490 (July 1993).

11. J. E. Field and A. Imamoglu, "Spontaneous Emission Into an Electromagnetically Induced Transparency," *Phys. Rev. A* **48**, 2486-2489 (September 1993).

DETAILED PROGRESS REPORT

Professor Richard N. Zare

Ion Imaging of Molecules Scattered from Surfaces

[Mark Ellison, Alan Furlan, and Carl Matthews]

During the past 12 months we have assembled a chamber for and demonstrated the feasibility of ion imaging as a detection technique in surface scattering experiments. Briefly, in such an experiment, a pulsed, chopped molecular beam impinges upon and scatters from a single crystal surface of a metal(see Figure 1). Scattered molecules are ionized by a pulsed laser and allowed to drift into the extraction region of the detector. In this region, a voltage pulse pushes the ions into a flight tube, at the end of which they strike a multi-channel plate/phosphor screen array. A CCD camera then captures the resulting image. The principal advantage of this detection technique is that a vast amount of information is obtained in just one image. As a result, the angular and velocity distributions of scattered molecules as a function of their internal quantum state can be determined. Currently, we are using this method to study the scattering of N_2 from Ni(111).

Much of the past 12 months have been spent assembling the chamber, aligning the molecular beam and ionizing laser, and generally eliminating all of the "little problems" that prevent the recording of meaningful data. An example of one of these "little problems" is presented in Figure 2. At low rotational quantum number, J, ions are detected only at the upper right of the phosphor screen. Conversely, at larger J, ions become visible at the lower left corner of the screen. We were elated at this "discovery", thinking that we were directly observing two distinct channels: direct scattering and trapping/desorption. Further investigation showed, however that the ion packet appearing in the upper right had precisely the same rotational population distribution as the incident molecular beam (see Figure 3). The presence of this ion packet can be attributed to an unanticipated electric field on the sample holder. Some molecules in the incoming beam are ionized before they strike the surface, and this field is sufficiently strong to deflect them back into the detector. Such an effect can obviously distort our results. Therefore, we are currently working to minimize, if not eliminate, all electric fields in the vicinity of our detector.

The ions observed at the lower left of the screen have, in fact, been scattered from the surface. Their rotational population distribution is shown in Figure 3. Note that these molecules are highly rotationally excited as compared to the incident molecular beam. A

rudimentary analysis of this distribution shows that the scattered molecules are rotationally slightly warmer than the surface temperature. This result, as evidenced by Figure 3, demonstrates that ion imaging can be applied as a detection technique to gas-surface interaction studies.

In summary, we have established the applicability of ion imaging to studies of the interactions of a gas with a single crystal surface. As discussed above, this detection technique promises to yield a great amount of information regarding the angular, velocity, and quantum state distributions of scattered molecules. After overcoming the remaining experimental obstacles, we will be poised to begin ion imaging experiments that further our understanding of gas-surface interactions.

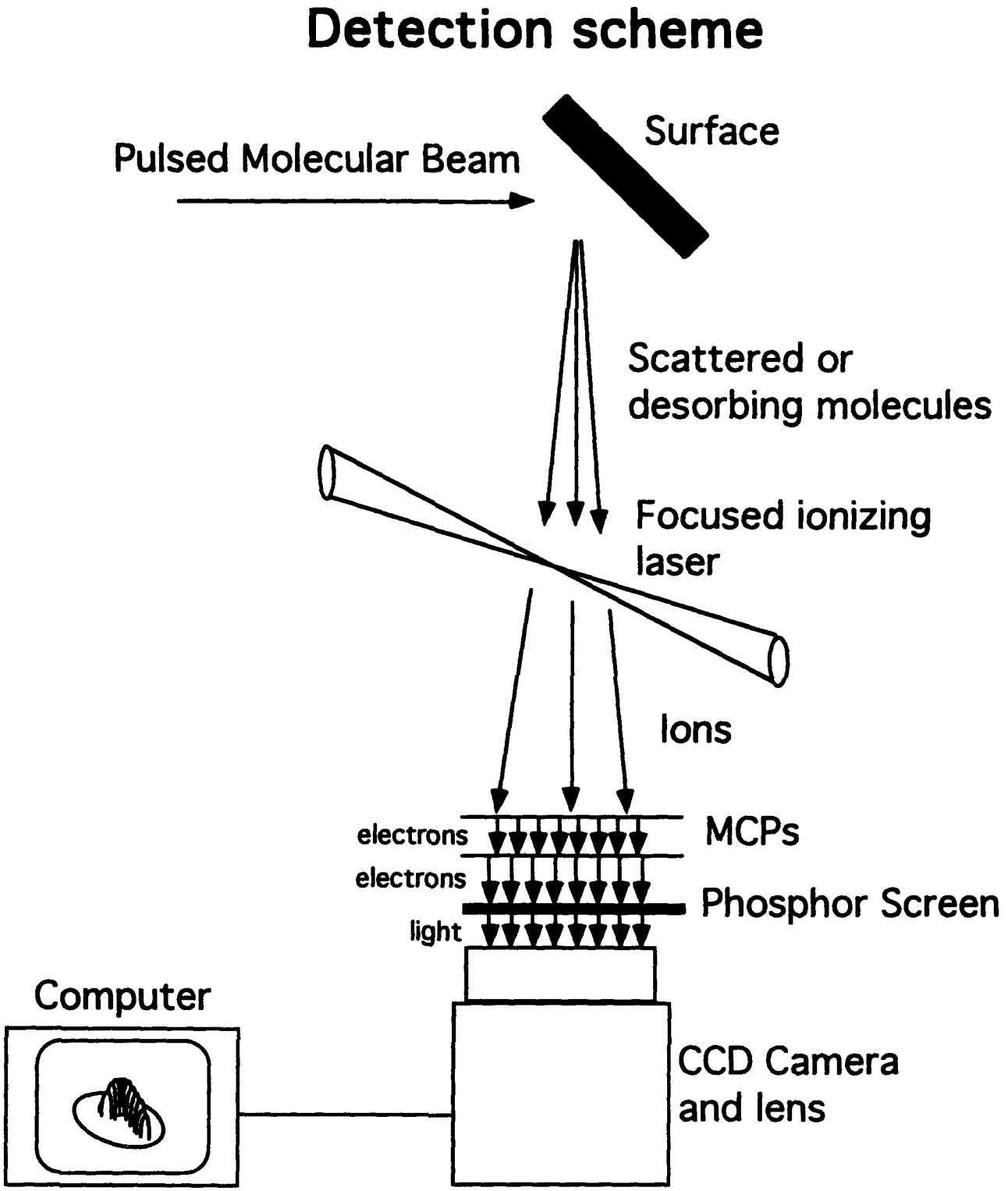

Figure 1. Schematic representation of experimental apparatus

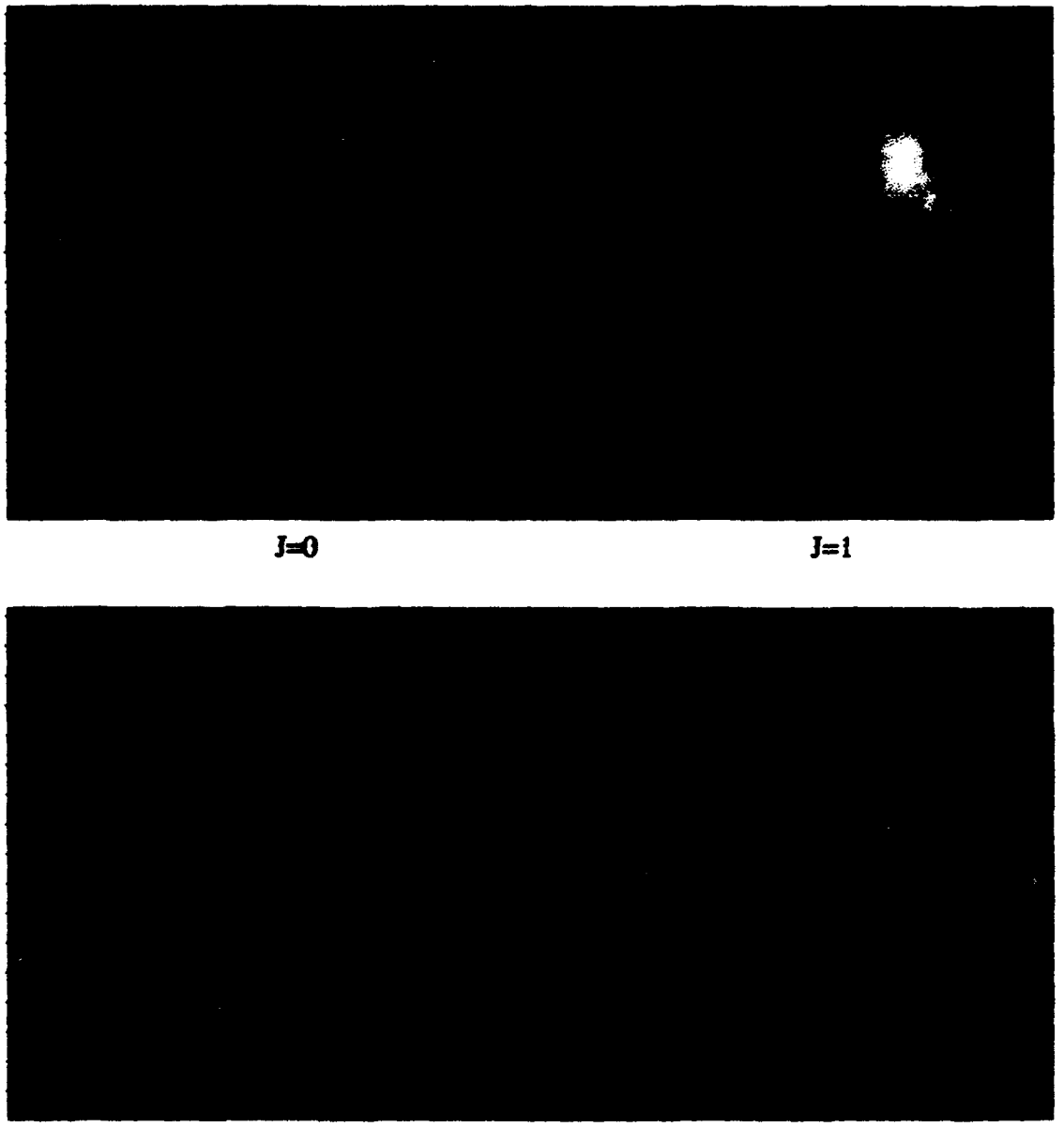

Figure 2. Rotational state dependence of "angular distribution"

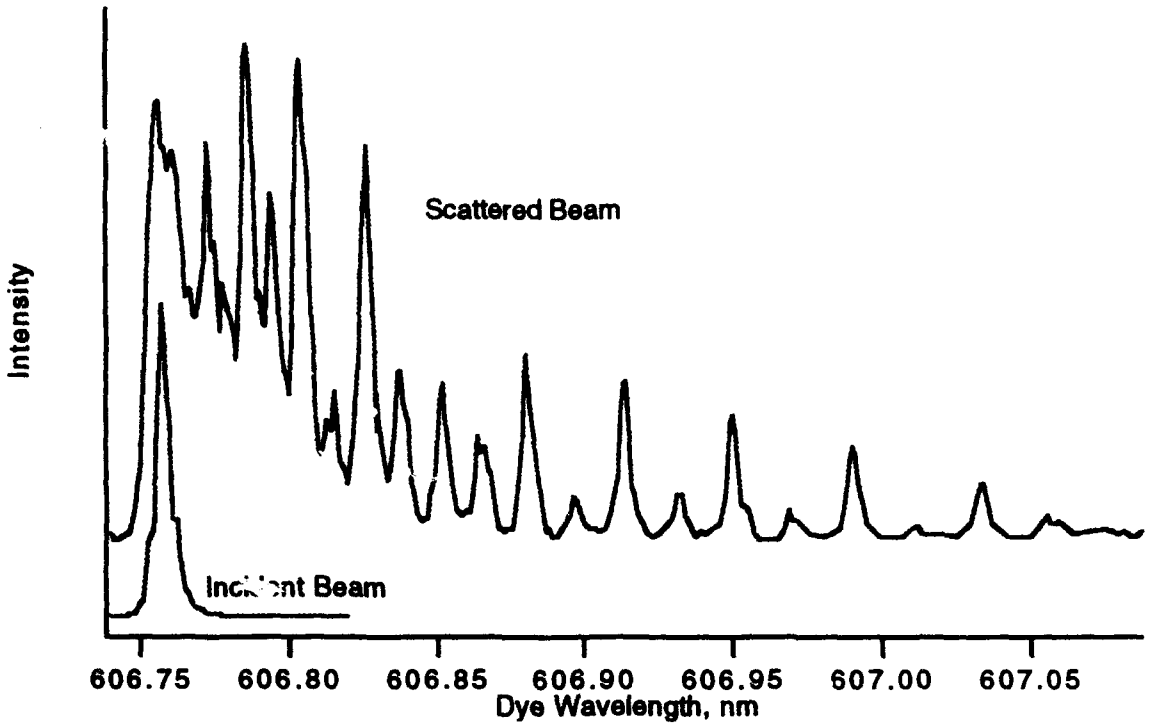

Figure 3. Rotational Population Distribution for Incident and Scattered Molecules

ONR Progress Report

A. L. Schawlow

July 1994

Weak absorption Lines in Opaque Solids, such as Metals

A theoretical study of the spectral line shapes for first-surface reflection from solids has been completed and submitted for publication. The analysis concerns the shapes of weak sharp lines observed in reflection from an isotropic solid with a general index of refraction. A combination of a simple semi-classical resonant index of refraction with a general background index is shown to result in a rich variation in line shapes. Argand diagrams are used as an aid in visualizing the origin and characteristics of these line shapes. Applications include reflection spectroscopy of ions and other centers in semiconducting and metallic solids.

Publications Spectral Line shapes for First-Surface Reflection from Solids, by B.W. Sterling, A.L. Schawlow and M.L. Jones, submitted to Journal of the Optical Society of America B.